To appear in AJ (April 2003 issue)

Near-infrared Spectra of Chamaeleon I Stars[1]

M. Gómez[2]

Observatorio Astronómico de Córdoba, Laprida 854, 5000 Córdoba, Argentina

mercedes@oac.uncor.edu

and

D. Mardones[2]

Departamento de Astronomía, Universidad de Chile, Casilla 36-D, Santiago, Chile

mardones@das.uchile.cl

ABSTRACT

We present low resolution (R $\sim$ 500) near-infrared spectra of 46 candidate young stellar objects in the Chamaeleon I star-forming region recently detected in several deep photometric surveys of the cloud. Most of these stars have $K <$ 12. In addition, we present spectra of 63 previously known southern hemisphere young stars mainly belonging to the Chamaeleon I and Lupus dark clouds. We describe near-infrared spectroscopic characteristics of these stars and use the water vapor indexes to derive spectral types for the new objects. Photometric data from the literature are used to estimate the bolometric luminosities of all sources. We apply D'Antona & Mazzitelli (1998) pre-main sequence evolutionary tracks and isocrones to derive masses and ages. We detect two objects with mass below the H burning limit among the 46 new candidates. One of this object (PMK99 IR Cha INa1) is the likely driving source of a bipolar outflow in the northern region of the cloud.

Combining our targets with previously known members of the cloud we analyze the mass and age distributions for 145 stars in the Chamaeleon I dark could. The mass histogram rises from about 2.5 M$\odot$ up to 0.4 M$\odot$ and then falls off. The median mass is 0.30 M$\odot$. The current population with masses $>$ 0.4 M$\odot$

[1]Based on observations collected at the European Southern Observatory, Chile, (ESO proposal N.63.I-0269(A)).

[2]Visiting Astronomer, Cerro Tololo Inter-American Observatory. CTIO is operated by AURA, Inc. under contract to the National Science Foundation.

is essentially complete. The scarcity of very low mass members is interpreted as population bias towards the least massive and fainter objects. If we assume the *true* Chamaeleon I IMF is flat (in logarithmic mass bins) in the interval 0.4 – 0.04 M$\odot$ as found by Comerón et al. (2000) in the central 300 arcmin^2 region, then we estimate that $\sim$ 100 stars remain to be found in that mass range. The distribution of ages indicates an active star-formation episode within the last $\sim$ 5×10^5 yr and a decreasing rate at older ages (few $\times$ 10^7 yr).

Subject headings: star: formation, star: pre-main sequence, star: low mass, brown dwarfs, star: HR diagram, ISM: individual (Chamaeleon I)

1. Introduction

In recent years there have been many infrared surveys of the Chamaeleon I dark cloud (Cambrésy et al. 1998; Persi et al. 1999; Oasa et al. 1999; Persi et al. 2000; Gómez & Kenyon 2001; Persi et al. 2001). These surveys provide many new candidate pre-main sequence stars based on photometric criteria. These observations aim to detect the faintest and thus the least massive pre-main sequence stars and are, in most cases, sensitive enough to detect young stars with masses close or even below the H burning limit. A complete census of the stellar population in the cloud would provide better estimates of the mass distribution and the star-formation history of Chamaeleon I. In particular, these surveys open the door to study the IMF down to the substellar regime. The Chamaeleon I cloud is especially adequate for these purposes since it is located nearby (**?**, d $\sim$ 160 pc,)]whi97, while also extending over moderate angular scales on the sky (**?**, $\sim$ 3 deg^2,)]bou98,miz01.

Lawson et al. (1996) determined the IMF of the cloud down to $\sim$0.3 M$\odot$ based on $\sim$ 80 optically visible known members and found a good agreement with the Miller-Scalo model. Comerón et al. (2000) intensively observed a small region (300 arcmin^2) in the center of Chamaeleon I dark cloud. This area contains 22 young stars, including 13 very low mass members with K $\sim$ 11–13.5 identified in Hα. They found that the IMF for the central area of the Chamaeleon I cloud was roughly flat (in logarithmic mass units) from $\sim$ 1 M$\odot$ down to $\sim$ 0.03 M$\odot$.

In order to study the extended low-mass IMF in the whole Chamaeleon I, it is desirable to determine characteristics of the new candidate young stars such as spectral types. The near-infrared spectra combined with published pre-main sequence evolutionary tracks can also be used to derive stellar masses and ages. In this contribution we present near-infrared spectra of 46 of the brightest (*typically* $K < 12$) candidate young stellar objects selected from the surveys cited above. We chose the brightest objects in order to have reasonable completeness and to achieve good S/N ratios in 4-m class telescopes.

In addition, we obtained near-infrared spectra of 63 previously known members of this

cloud as well as other nearby southern star-forming regions such as Lupus. We used these known young stellar objects as a spectral type calibration group. These known objects and the Greene & Lada (1996) atlas allow us to identify spectroscopic features usually present in young stellar objects that support the pre-main sequence status of the new objects. We combine our data with published photometry and spectral types of other sources in the cloud to compile a list of 145 pre-main sequence stars in the Chamaeleon I dark cloud and study the mass and age distributions.

In §2 we describe the observations and data reduction. In §3 we present our analysis and results. We derive spectral types from the water vapor indexes which combined with published photometry allows us to place the stars in the HR diagram. We conclude with a brief summary in §4.

2. Observations and Data Reduction

We carried out these observations on April 10 – 12, 1999 with the ESO NTT near-infrared spectrograph/imaging camera SOFI (Son OF ISAAC) and on May 6 – 9, 1999 with OSIRIS (Ohio State Infrared Imager and Spectrometer) on the CTIO Blanco 4-m telescope. A few additional spectra were obtained on Feb 27 –28, 2002 with this telescope and infrared camera. Tables 1 and 2 list the targets observed.

SOFI has two low resolution grisms (red and blue) that roughly cover the JHK bands on a Hawaii HgCdTe 1024×1024 detector with a plate scale of 0.292″/pix. The blue grism covers the spectral region between 0.95–1.63 μm and the red grism the region between 1.53–2.52 μm. The corresponding spectral resolutions (R = $\lambda/\Delta\lambda$) are 930 and 980 for a 0.6″ slit. We used a 1″ wide and 290″ long slit. OSIRIS was used in the X-Disp (multi-order/cross-dispersed) mode with the f/2.8 camera and a slit 30″ long and 1.2″ wide. This configuration gives R ($\lambda/\Delta\lambda$) $\sim$ 1200 (2 pixels), while covering the J, H, and K bands simultaneously on a 1024 × 1024 HgCdTe detector at a plate scale of 0.403″/pix[3]. In particular, the X-Disp mode uses a cross-dispersing grism that gives the JHK spectral region in three adjacent orders, from 5th to 3rd.

The integration time and the number of exposures per target were chosen based on the brightness of the source and background contribution each night. In most cases we obtained two sets of 9 blue and red spectra of the same integration time with SOFI. We repeated this sequence for objects fainter than $K = 13$. Common integration times were 90–180 sec for both grisms. The telescope was nodded 30–60″ along the 290″ long slit between consecutive positions following the usual ABBA pattern. This procedure corresponds to the "Nod Throw

[3]A full description of this instrument and its various configurations can be found at http://www.ctio.noao.edu/instruments/ir-instruments/osiris/index.html.

Along Slit" scheme as described in the SOFI Users Manual (Lidman et al. 2000). With OSIRIS we *typically* obtained seven images of identical integration time, with the telescope dithered by 7″ along the 30″ long slit. The individual integration times varied between 30 and 180 sec. For faint objects (i.e., $K > 12$) we obtained two 180 sec sequences of seven spectra.

In addition to the program sources we observed several atmospheric standards. We selected two groups of standards with similar airmass to our candidate sources and observed them (every ~ 2 hours) each night. These telluric stars comprise both late (G3-5) and early (O8) spectral types and were chosen from the lists available at both observing sites.

We obtained multiple flat field images, with a dome screen, using incandescent lamps on and off. A Xenon lamp, also taken on and off, each night provided the wavelength calibration for our SOFI data. To determine the wavelength scale of the OSIRIS spectra we used a HeNeAr lamp.

To reduce the data we used IRAF[4]. We subtracted one image from another (using pairs of nodded observations) to eliminate the background and sky contribution in first approximation. This subtraction automatically took care of dark current and bias level. We flat-fielded our data dividing by a normalized dome flat.

We used the *twodspec* task APALL to trace and extract the spectra along a 6 pixel wide aperture in the SOFI data and 10 pixel in the OSIRIS co-added images. In particular for OSIRIS data we treated JHK X-Disp adjacent orders using the *echelle* package. A further sky subtraction was done by fitting a polynomial to the regions on either side of the aperture. A non linear low order fit to the lines in the Xenon and HeNeAr lamps were used to wavelength calibrate the spectra.

We removed telluric features from our data dividing each program star by the atmospheric standard spectrum. For the OSIRIS data we used a G3-5 standard and both G3-5 and O8 stars for the SOFI spectra. The telluric star differed from the science target by $<$ 0.2 in airmass. We used the *onedspec* task SPLOT to remove H I (Paschen and Brackett) lines from the spectra of the G3-5 and O8 stars, interpolating across each line. The division by the standard canceled out telluric features in the science spectrum reasonably well but introduced the inverse of the atmospheric standard in the corrected spectrum. We recovered the true spectral shape multiplying the resultant spectrum by a Planck function at the temperature corresponding to the atmospheric star.

We finally combined the JHK X-Disp orders for our OSIRIS spectra and the blue and the red grism regions for each object observed with SOFI and eliminated regions of deep

[4]IRAF is distributed by the National Optical Astronomy Observatory, which is operated by the Association of Universities for Research in Astronomy, Inc. under contract to the National Science Foundation.

atmospheric absorptions. We also trimmed out wavelengths 0.95–0.97 μm from our SOFI spectra due to edge effects. The useful spectral range provided by OSIRIS is 12000-23500 Å while SOFI covers from 9700 to 25300 Å. For the SOFI spectra, as mentioned before, we obtained two sets of spectra corresponding to the G3-5 and O8 telluric stars that were essentially identical. In Section 3.2 we show the set of science spectra obtained applying the O8 standard as telluric corrector.

3. Data Analysis and Results

3.1. The Sample

We observed two groups of stars: a) 46 candidate young stellar objects detected by several recent surveys of the cloud; and b) 63 previously known young stars (36 belonging to the Chamaeleon I dark cloud and 27 located in other star-forming regions, such as Lupus). Three objects in the second group (VW Cha, SZ 119, and SZ 124) were observed with both SOFI and OSIRIS. Eight of the stars in the second group already had near-infrared spectra. Greene & Lada (1996) observed Haro1-1 in the ρ Ophiuchi cloud and Gómez & Persi (2002) CCE98 49 (ISO-ChaI 256) in Chamaeleon I. Comerón et al. (1999) published combined HK band spectra for Cha Hα 1–6. Gómez & Persi (2002) obtained individual JHK band spectra for Cha Hα 1 and Cha Hα 2. In this paper we report individual JHK data for each of the Cha Hα 1–6 stars.

The 46 new objects were selected, in general, among the brightest (*typically* K < 12) near-infrared objects detected by several recent surveys in the cloud (Cambrésy et al. 1998; Persi et al. 1999; Oasa et al. 1999; Persi et al. 2000; Gómez & Kenyon 2001; Persi et al. 2001). These lists include about ~ 150 additional potential members of the cloud with K $>$ 13. In this contribution we analyze data for the brightest objects for which it is feasible to obtain near-infrared spectra with a 3-4 meter class telescope in about 20-40 minutes total integration time.

The second set of 63 previously known objects were selected among the southern hemisphere pre-main sequence stars to have a group of reference from which to derive common near-infrared spectroscopic features among young stellar objects. Objects with previously known spectral types within this group allowed us to calibrate the water vapor index I_{H_2O} based classification (see section 3.4).

3.2. The Near-infrared $H-K$ vs $J-H$ Diagram

Tables 3 and 4 compile photometric and spectroscopic data (when available) for the observed stars. Figure 1 shows the position of new (stars) and previously known (dots)

objects in the near-infrared color-color diagram. Superposed on this plot are the loci of unreddened main sequence dwarfs (**?**, solid line,)]bebr88 and CTTS –classical T Tauri stars– (**?**, long-dash line,)]mey97. The reddening band (**?**, dotted line,)]goke01 and the length of the reddening vector (Rieke & Lebofsky 1985) are also indicated.

Although some of the candidate objects have significant near-infrared excesses indicating the presence of circumstellar material, most of the previously known and new sources are located within or close to the reddening band. The group of known objects includes many bona-fide CTTS in the cloud (**?**, e.g.,)]gast92,com00 without measurable near-infrared excesses and thus the near-infrared color-color diagram may miss a significant number of young members of the cloud. Most of the candidate sources located within the reddening band in Figure 1 were proposed by Cambrésy et al. (1998) based on the $I - J$ vs $J - K$ diagram. Near-infrared spectra provide additional information to support the pre-main sequence nature of these candidate sources.

3.3. The Spectra

Figure 2 shows the JHK band spectra of all candidate objects reported in this paper and Figure 3 a selected sub-sample of 12 of the previously known young stellar objects we observed [5]. Prominent atomic and molecular features in the observed spectral range for late type stars (i.e., spectral types later than G0) are labeled (Kleinmann & Hall 1986; Wallace et al. 2000; Meyer et al. 1998; Wallace & Hinkle 1997). Both groups (new objects –Figure 2– and previously known young stars –Figure 3–) have a wide variety of spectral shapes. Some sources have shapes decreasing with λ, others display a turnover around 1.6–1.8 μm or the spectral shape is roughly constant. Other objects have rising or steeply rising shapes towards 2 μm. Considered as groups, new young stellar objects and previously known stars show similar near-infrared spectroscopic characteristics.

Greene & Lada (1996) presented an atlas of low resolution spectra of $\sim$ 100 young stellar objects in different star-forming regions, including Taurus, ρ Ophiuchi, R Cra, IC 5146, Scorpio, and Lupus. These authors describe near-infrared spectroscopic characteristics of class I, II, and III objects as well as flat-spectrum and FU Orionis objects. They found that, in general, the spectral shapes correlate with the spectral energy distribution class and that equivalent widths of absorption features decrease from the class III to the class I sources, as a consequence of the increasing amount of circumstellar material. In addition many young stellar objects (usually class II and I) have atomic hydrogen lines in emission.

For the previously known young stellar objects observed we find a similar correlation

[5]The spectra of the remanding 51 known stars as well as those shown in Figures 2 and 3 are available upon request to the authors.

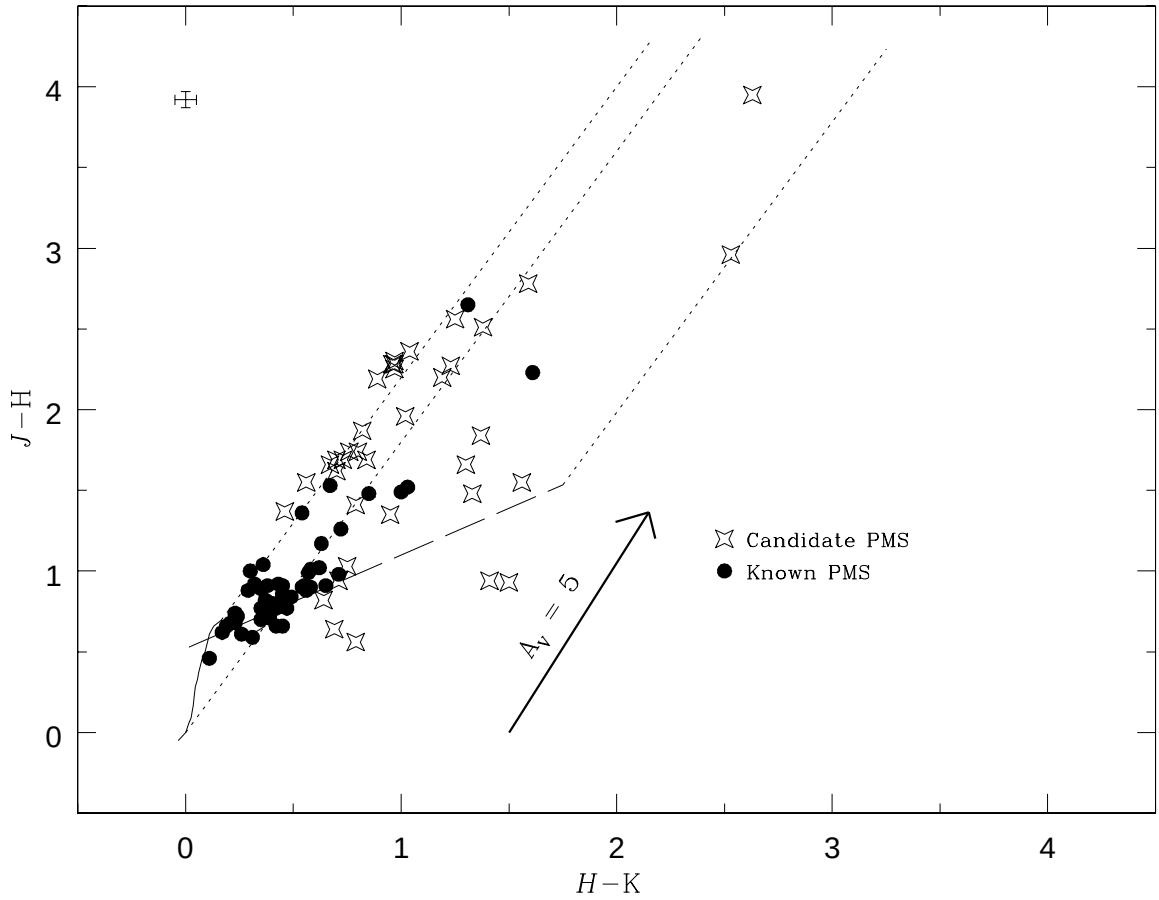

Fig. 1.— Near-infrared color-color diagram for the candidate (stars) and previously known (dots) sources listed in Tables 3 & 4. The solid and long-dash lines indicate the loci of unreddened main sequence dwarfs (Bessell & Brett 1988) and CTTS (Meyer et al. 1997). The dotted lines define the reddening band, corresponding to a reddening vector $E(J-H)/E(H-K) = 1.80$ (Gómez & Kenyon 2001). The arrow indicates an $A_V = 5$ mag (Rieke & Lebofsky 1985). Typical photometric errors are displayed in the upper left corner.

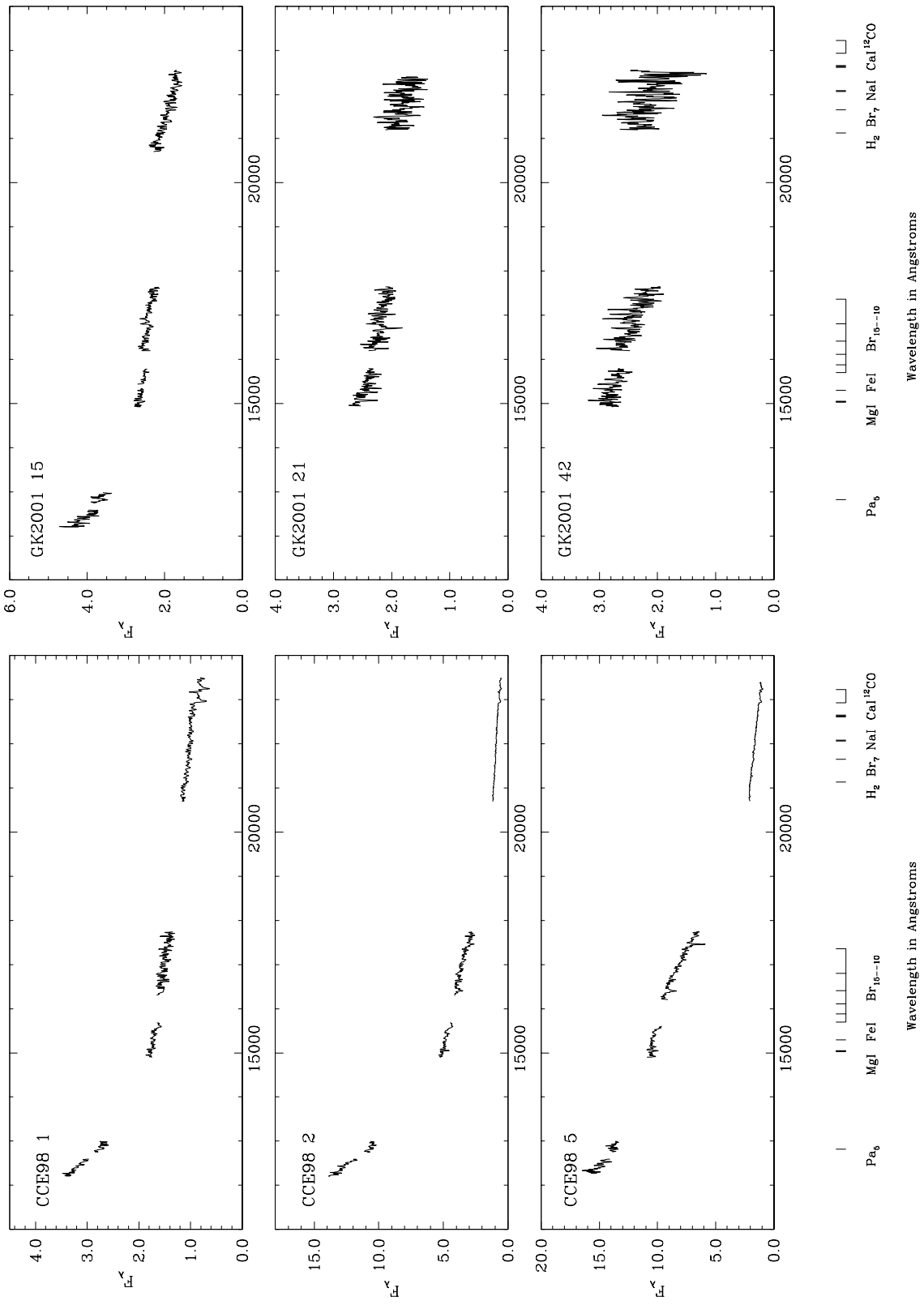
GK2001 15
GK2001 21
GK2001 42
CCE98 1
CCE98 2
CCE98 5
F_λ
Wavelength in Angstroms
Pa_δ
MgI FeI
Br_{15-10}
H_2 Br_γ NaI $CaI^{12}CO$

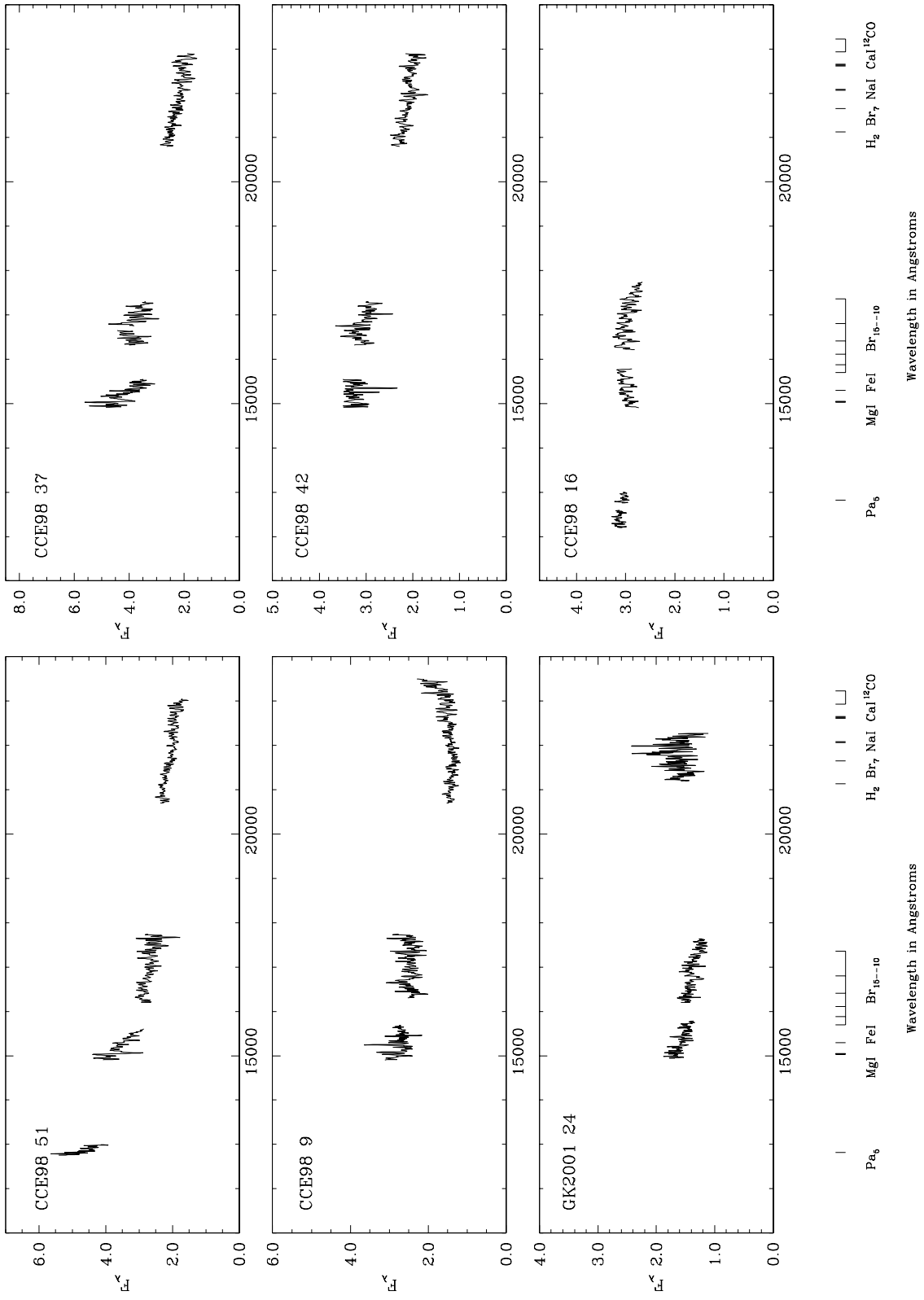
CCE98 37
CCE98 42
CCE98 16
CCE98 51
CCE98 9
GK2001 24
F_λ
Wavelength in Angstroms
Pa_δ
MgI FeI
Br_{15-10}
H_2 Br_7 NaI $CaI^{12}CO$

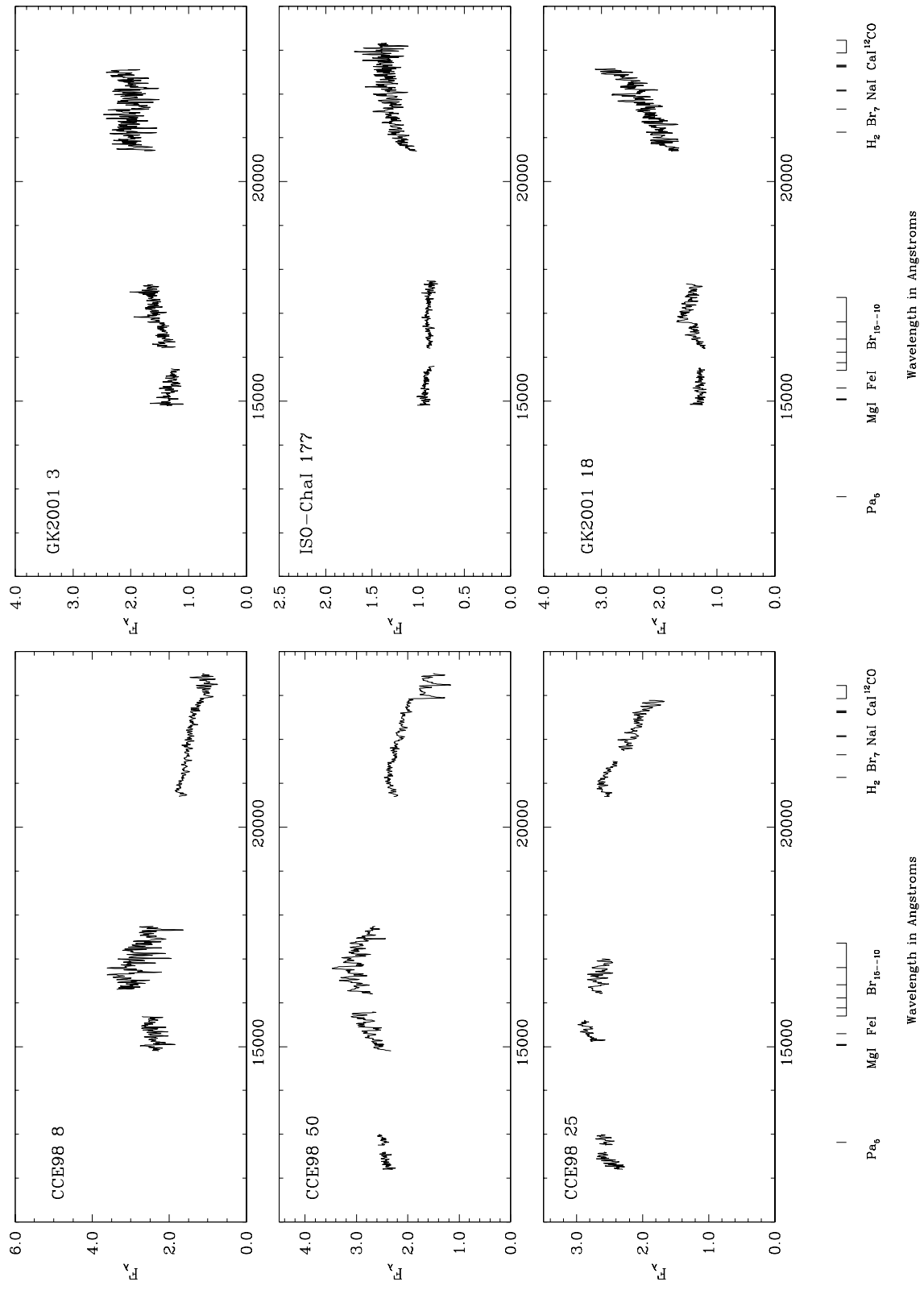
CCE98 8
CCE98 50
CCE98 25
GK2001 3
ISO−Cha1 177
GK2001 18
F_λ
Wavelength in Angstroms
Pa_δ
MgI FeI Br_{15-10}
H_2 Br_γ NaI $CaI^{12}CO$

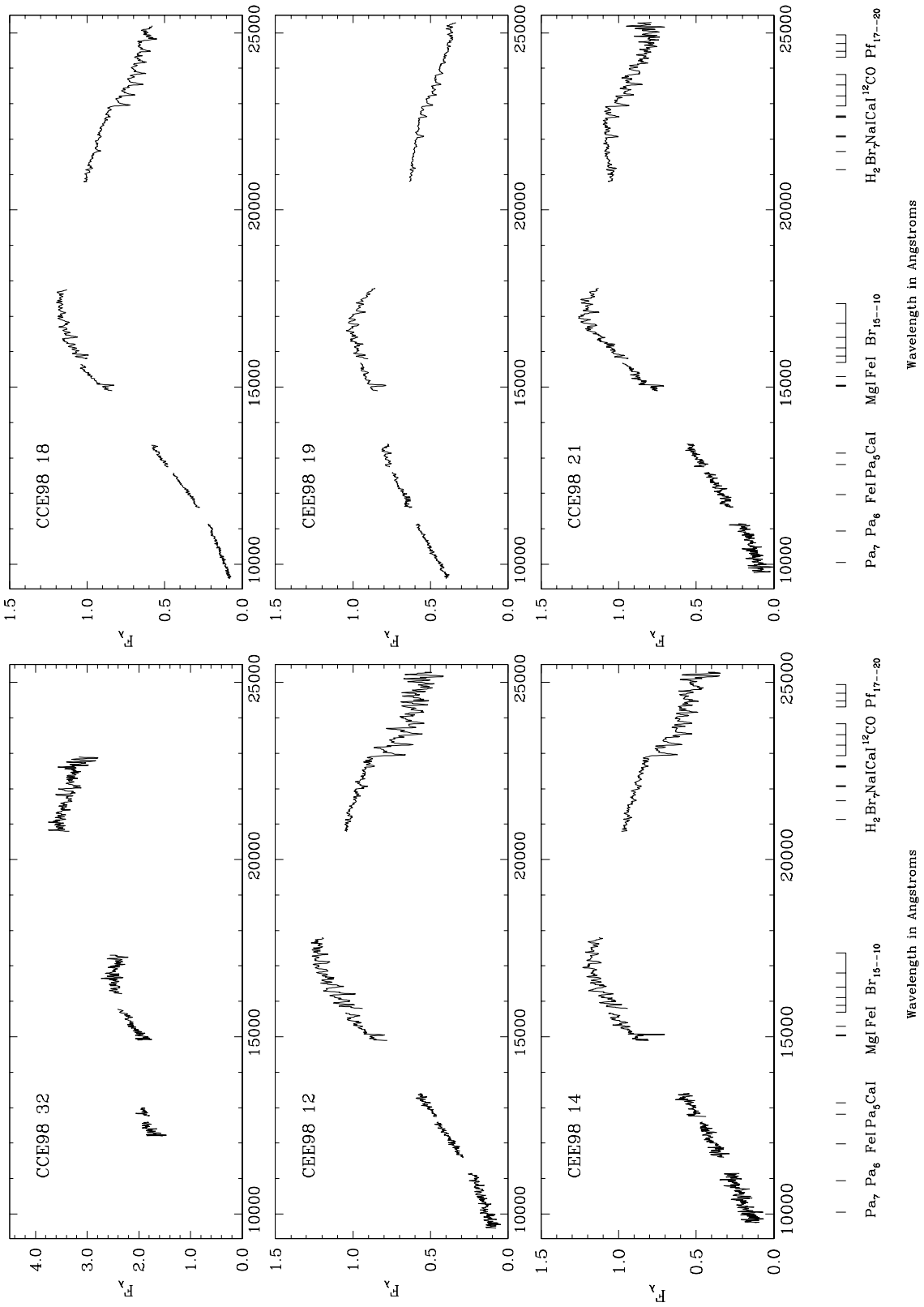
CCE98 32
CCE98 18
CEE98 12
CEE98 19
CEE98 14
CCE98 21
F_λ
Wavelength in Angstroms
Pa_7 Pa_6 FeI Pa_5CaI MgI FeI Br_{15-10} H_2 Br_7NaICaI ^{12}CO Pf_{17-20}

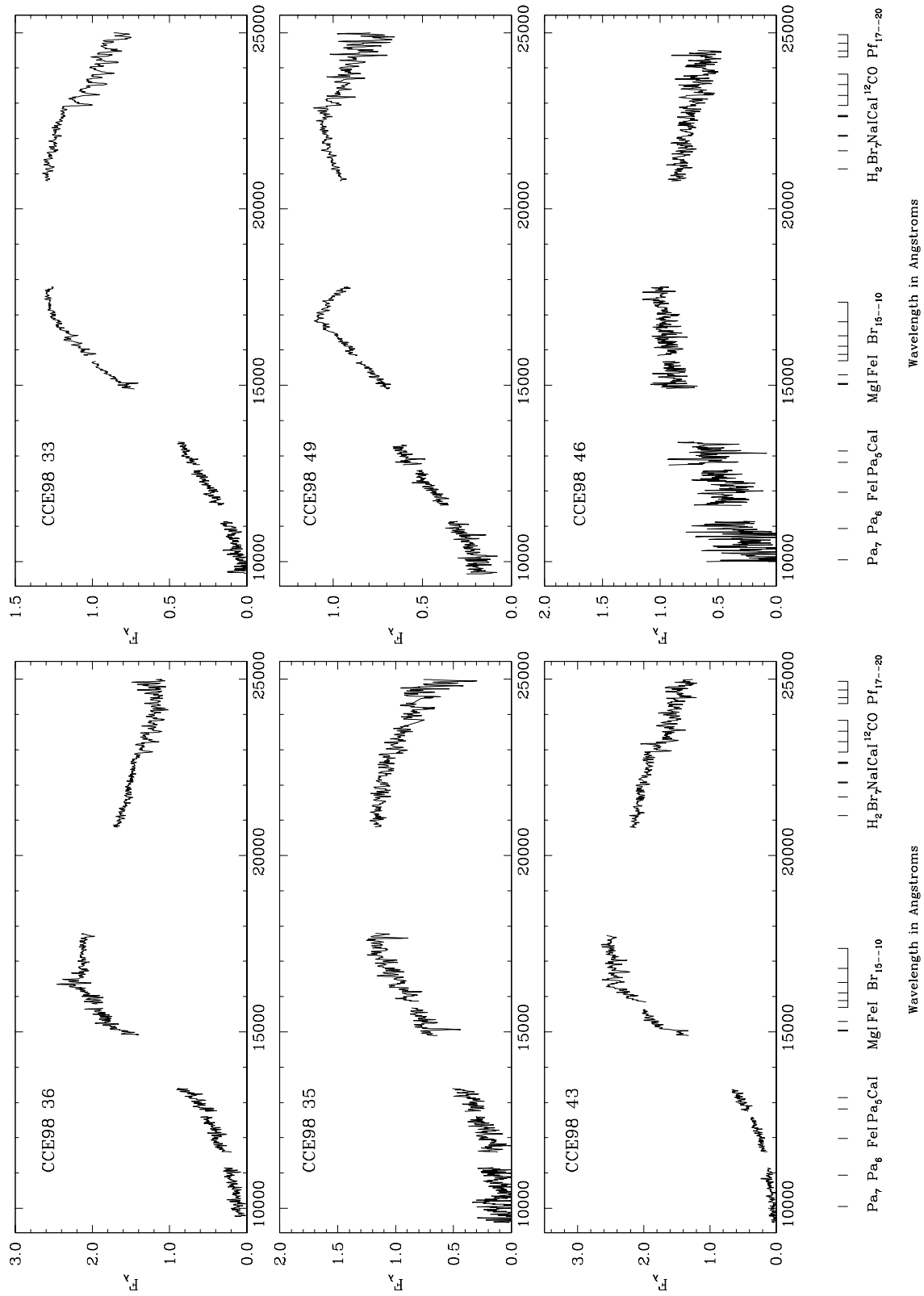
CCE98 33
CCE98 49
CCE98 36
CCE98 35
CCE98 46
CCE98 43
F_λ
Wavelength in Angstroms
Pa_7 Pa_6 FeI Pa_5CaI MgI FeI Br_{15-10} H_2Br_7NaICaI ^{12}CO Pf_{17-20}

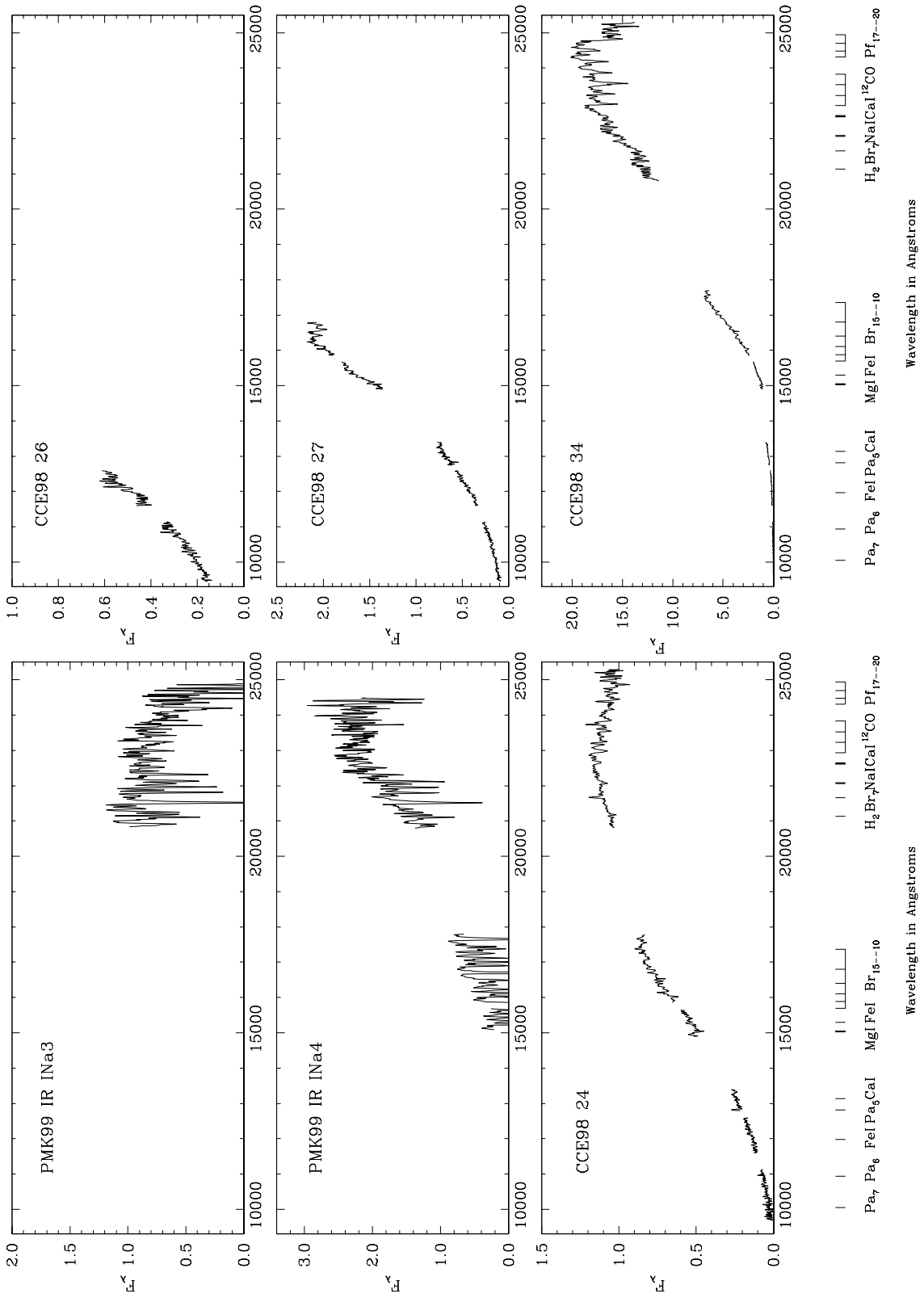
PMK99 IR lNa3
PMK99 IR lNa4
CCE98 24
CCE98 26
CCE98 27
CCE98 34
F_λ
Wavelength in Angstroms
Pa_7 Pa_6 FeI Pa_5CaI MgI FeI Br_{15-10} H_2 Br_7NaICaI ^{12}CO Pf_{17-20}

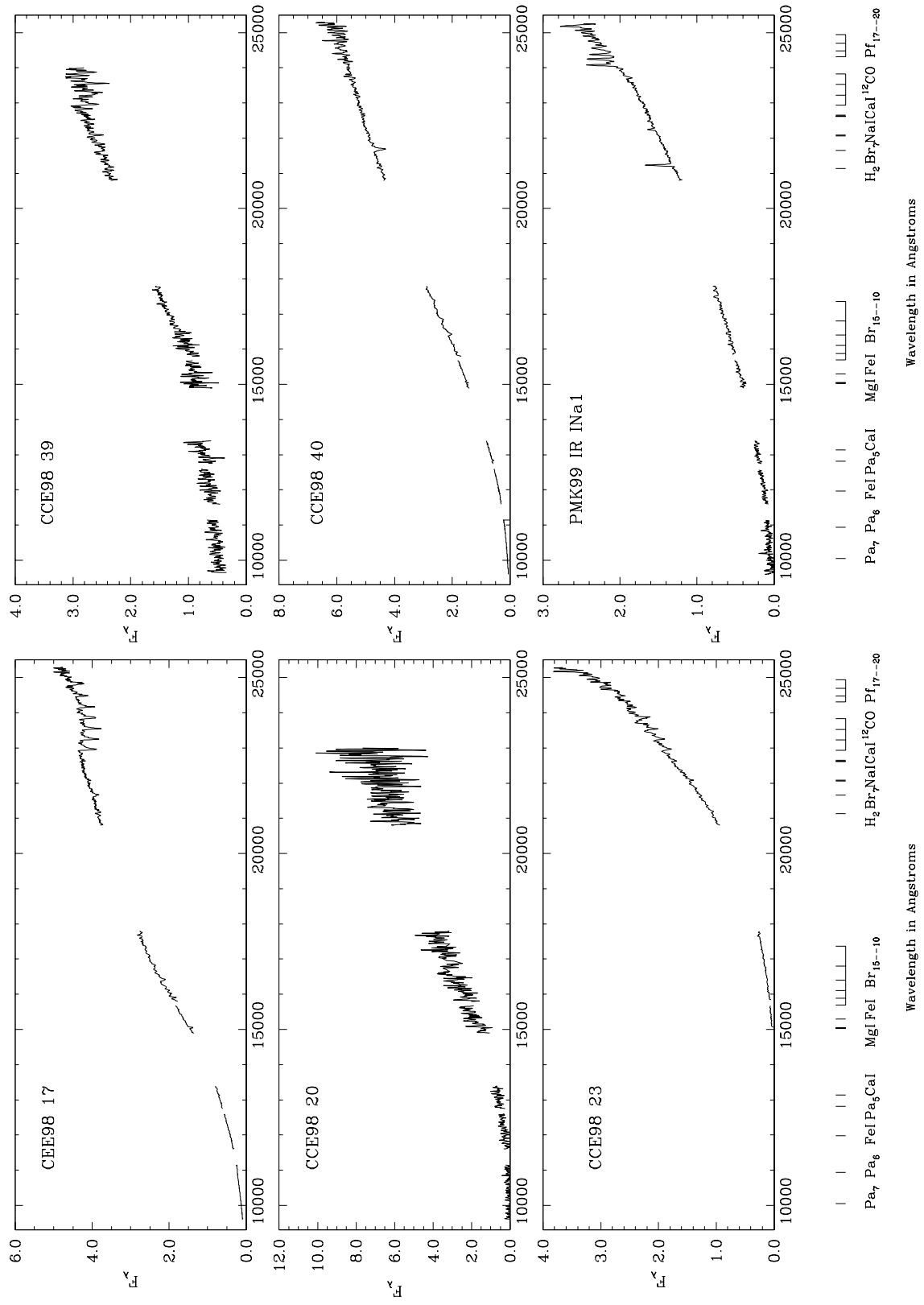
CCE98 17
CCE98 20
CCE98 23
CCE98 39
CCE98 40
PMK99 IR INa1
F_λ
Wavelength in Angstroms
Pa_7 Pa_6 FeI Pa_5CaI
MgI FeI Br_{15-10}
H_2Br_7NaICaI^{12}CO Pf_{17-20}

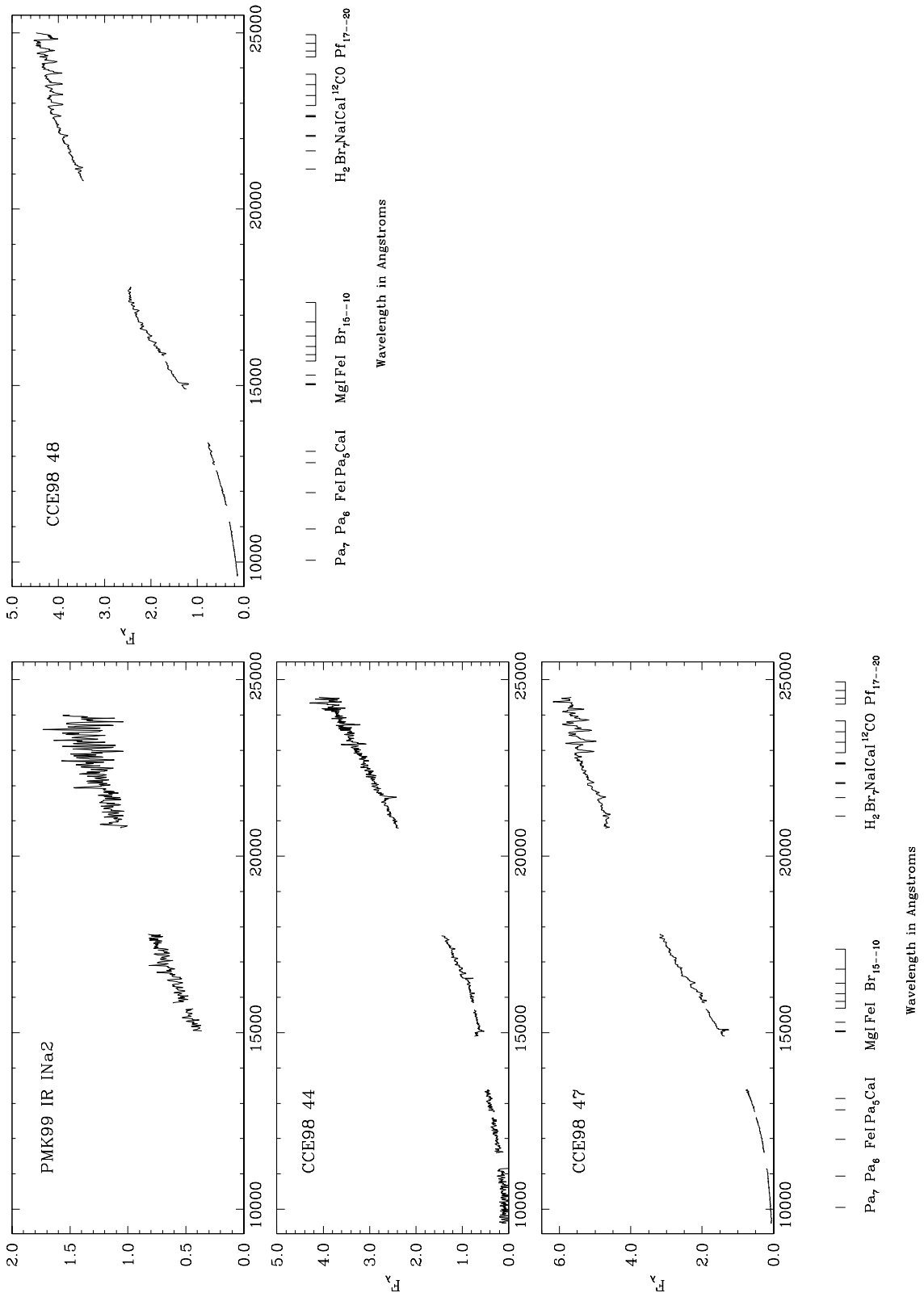

Fig. 2.— *JHK* band spectra of candidate young stellar objects in the Chamaeleon I dark. Prominent atomic and molecular features in the observed spectral range are labeled.

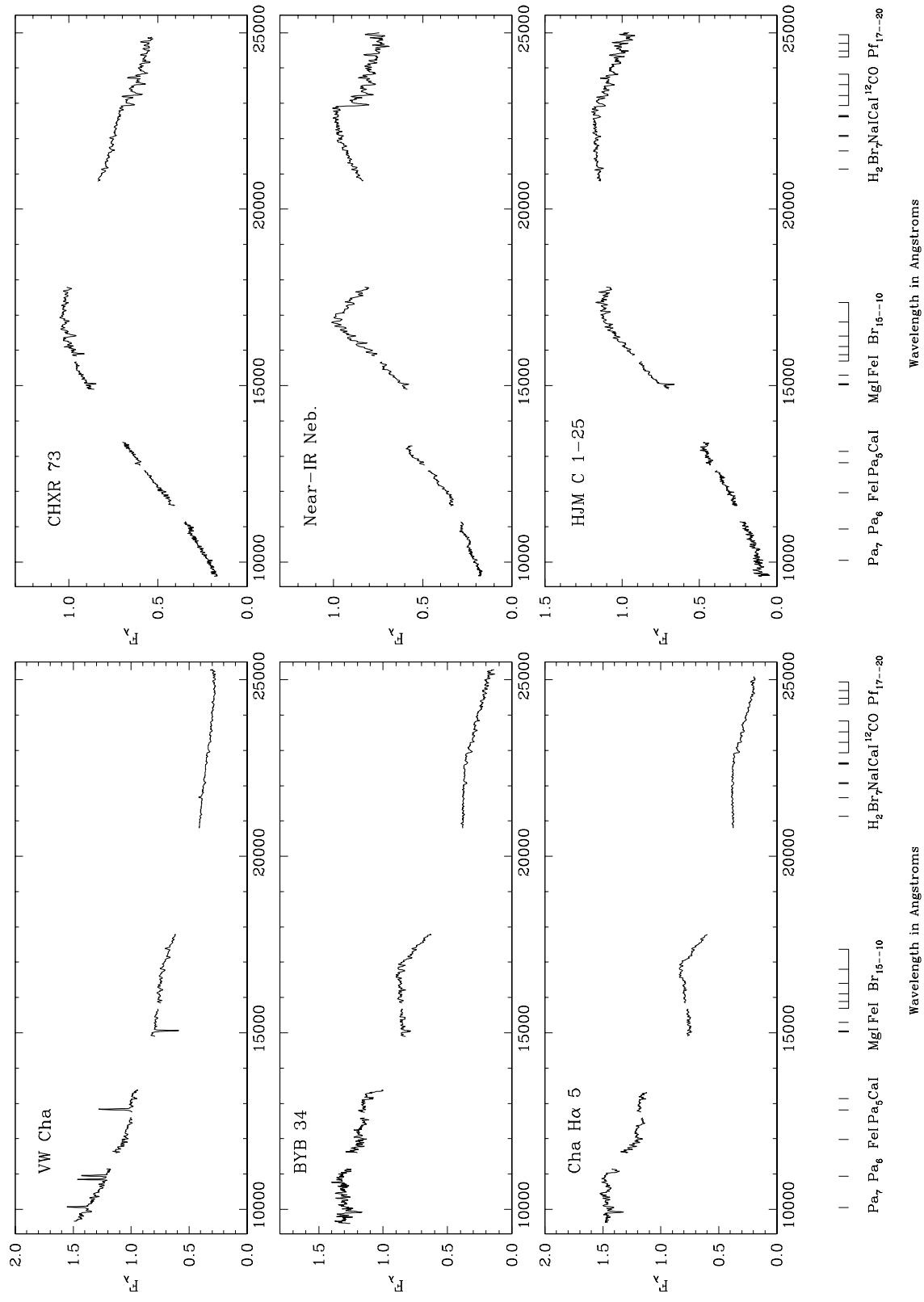
VW Cha
CHXR 73
BYB 34
Near−IR Neb.
Cha Hα 5
HJM C 1−25
F_λ
Wavelength in Angstroms
Pa_7 Pa_6 FeI Pa_5CaI MgI FeI Br_{15-10} H_2Br_7NaICaI ^{12}CO Pf_{17-20}

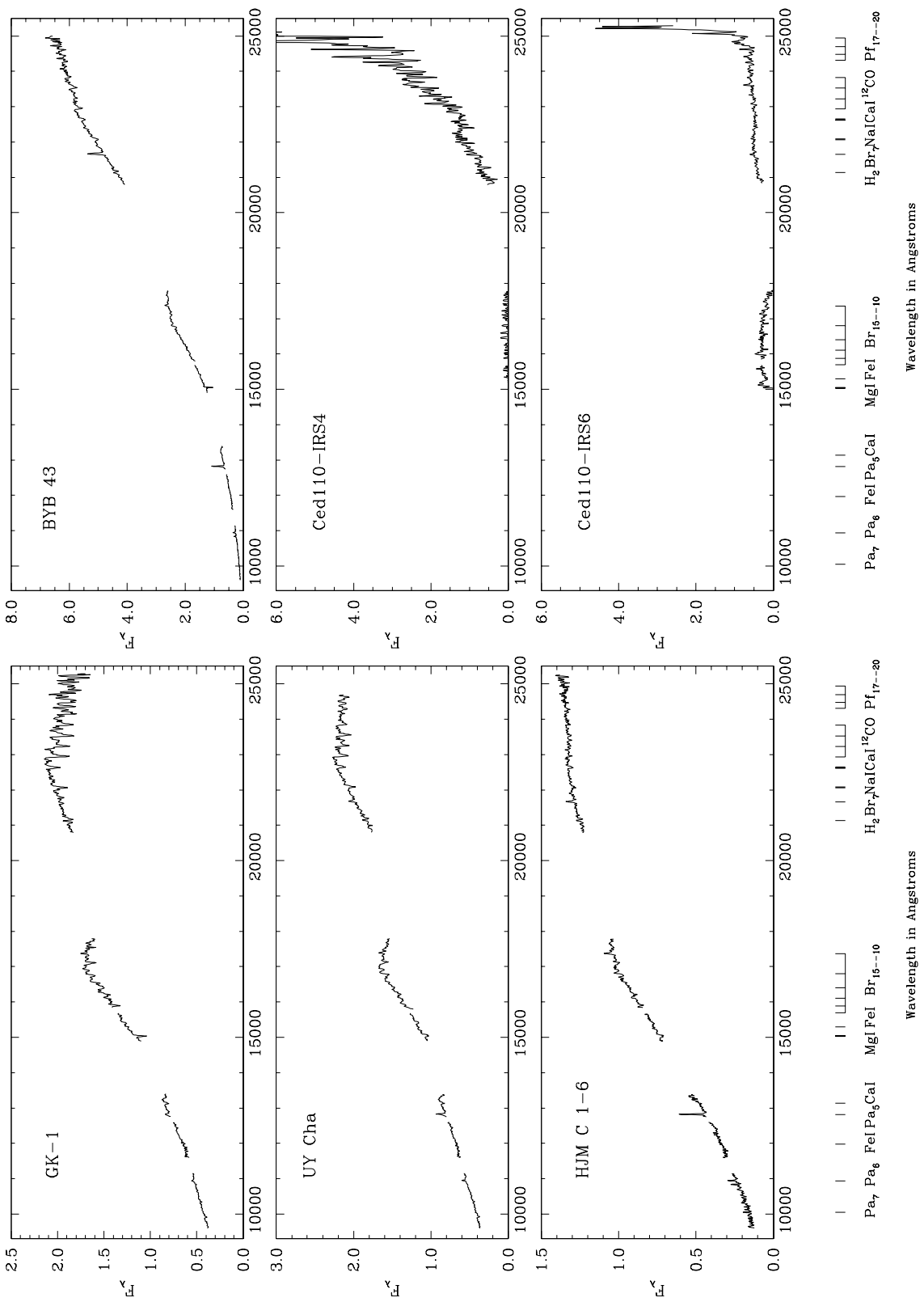

Fig. 3.— JHK band spectra of 12 of the previously known young stellar objects for which we obtained near-infrared data. Prominent atomic and molecular features in the observed spectral range are labeled.

between the spectral shape and the classical (class II) or weak emission (class III) T Tauri type. In general, class II objects have rising or flat spectral shapes. Class III stars have decreasing or flat spectral shapes. We find candidate sources have rising, flat, and decreasing shapes. The first and second groups probably correspond to class I-II members of the cloud and the rest to potential class III young stellar objects.

Tables 5 and 6 list equivalent widths corresponding to the strongest lines detected in the spectra of the observed targets. For the SOFI data we estimate an uncertainty of $\sim$ 1-2 Å in the Paβ, Brγ, Na I doublet (2.206 and 2.209 μm), and Ca I triplet (2.261, 2,263, and 2.266 μm) equivalent widths. The combined CO ν = 2-0 and 3-1 bands have a slightly worse precision of $\sim$ 3 Å. The OSIRIS spectra in general have poorer S/N ratio in relation to SOFI data. We estimate an error of 2-3 Å in our measurements of Paβ, Brγ, Na I doublet, and Ca I triplet. The OSIRIS spectra only cover CO ν = 2-0, and 3-1 bands. We estimate an uncertainty of $\sim$ 4-5 Å in the two CO bands covered by this instrument. The three stars observed with both instruments (VW Cha, SZ 119, and SZ 124) have equivalent width measurements that agree within the estimated uncertainties. We notice the SOFI spectra cover the four CO ν = 2-0, 3-1, 4-3, and 5-3 bands. In Tables 5 and 6 we provide the combine CO equivalent width corresponding to the ν = 2-0 and 3-1 bands to properly compare these measurements with those obtained for the OSIRIS data.

Stars in Tables 5 and 6 have, on average, similar or slightly smaller equivalent widths than M type standards (Kleinmann & Hall 1986; Wallace et al. 2000), with exception of few sources (such as PMK99 IR Cha INa1, Ced 110 IRS 4, Ced 110 IRS 6, and Glass I) with no absorption lines present, at the spectral resolution used. Greene & Lada (1996) also noticed that many young stellar objects in their sample (about 100 stars belonging to ρ Oph, Taurus, and other star-forming regions) have atomic (Na I and Ca I) and CO equivalent widths in the same range as late-type MK standards.

Figure 4 shows the Ca I vs Na I equivalent widths for the groups of previously known class II (CTTS) and class III (WTTS) objects observed. For the Ca I line equivalent width we obtain an average of 3.30 $\pm$ 1.39 and 4.88 $\pm$ 1.59 for the class II and class III, respectively. The Na I line equivalent width gives similar results: 3.48 $\pm$ 1.59 for the CTTS and 3.87 $\pm$ 1.32 for the WTTS. Although the uncertainties are large, on average, the class II sources have slightly smaller equivalent widths compared to the class III group. Smaller equivalent widths may indicate the presence of circumstellar material partially filling-in these absorption lines. A similar plot for the new sources gives only a marginal correlation between the equivalent widths and the spectral shapes. We note that the poor S/N ratio in the spectra of several candidate objects rendered uncertain the detection of spectral line features. Better S/N data are required to confirm this initial correlation.

Several stars (such as CCE98 24, VW Cha, HJC C 1-6, and BYB 43) also show H atomic lines in emission; the strongest are Paβ and Brγ. We notice an apparent tendency of a higher frequency of H I emission lines among previously known young stellar objects than

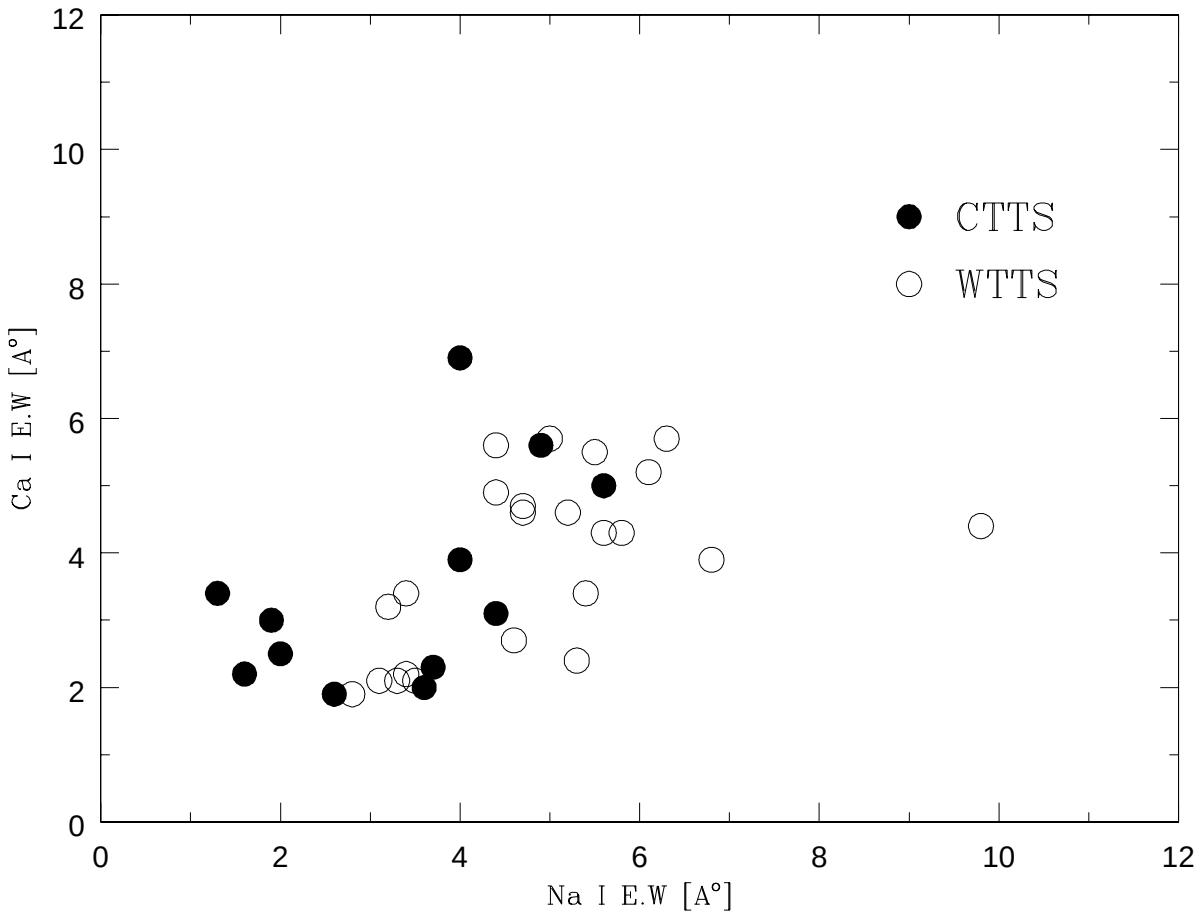

Fig. 4.— Ca I vs Na I equivalent widths (in Å) for previously known class II (CTTS) and class III (WTTS) sources.

among the new sources. Twenty of the 63 previously known young stars have Paβ or Brγ in emission, whereas only one of the 29 measured candidate young stars shows these features. However the modest S/N ratio of some of the new stars spectra may explain at least in part this tendency. Higher S/N data are necessary to properly consider this issue.

3.3.1. The PMK99 IR Cha INa1 Spectrum

Figure 5 shows an enlarged spectrum of the source PMK99 IR Cha INa1, that has molecular hydrogen in emission. In particular H_2 1-0 Q (1–8) as well as H_2 1-0 S (1–0) are clearly detected. PMK99 IR Cha INa1 is a class I source in the cloud identified by Persi et al. (1999) roughly located at the center of the high velocity bipolar outflow found by Mattila et al. (1989). Based on the physical properties of PMK99 IR Cha INa1 (steep spectral energy distribution and association with a small near-infrared nebula) Persi et al. (1999) proposed this star rather than HM 23 (a class II source lying in the region) as the exciting source of the bipolar outflow. HM 23 had been originally associated with the CO flow as it was the nearest young star known in the vicinity of the flow. Molecular hydrogen lines in the spectrum of PMK99 IR Cha INa1 are probably originated in the shock regions where bipolar outflow impacts on the surrounding molecular gas (Burton et al. 1989; Eislöffel et al. 2000; Rosenthal et al. 2000).

3.4. Spectral Type

To derive spectral types for the candidate sources we applied the stellar water vapor indexes proposed by Wilking et al. (1999) and Comerón et al. (2000). These indexes are reddening-free and compare the intensity of the absorption bands near 2 and 1.9 μm, respectively. The strength of these bands are extremely sensitive to the spectral types for M dwarfs. Wilking et al. (1999)'s index Q is defined by the average values of relative flux density calculated in three narrow bands, F1 (2.07–2.13 μm), F2(2.267–2.285 μm), and F3(2.40–2.50 μm), as

$$Q = (\mathrm{F1/F2})(\mathrm{F3/F2})^{1.22}. \quad (1)$$

This index can only be applied to the SOFI spectra. OSIRIS data have poor S/N ratio at wavelengths longer than 23500 Å.

The index I_{H_2O} (Comerón et al. 2000) measures the relative fluxes in four narrow band filters (0.05 μm width) centered at 1.675 μm, 1.750 μm, 2.075 μm, and 2.25 μm. Denoting the fluxes at each narrow band filter by f1, f2, f3, and f4, respectively, the index I_{H_2O} is

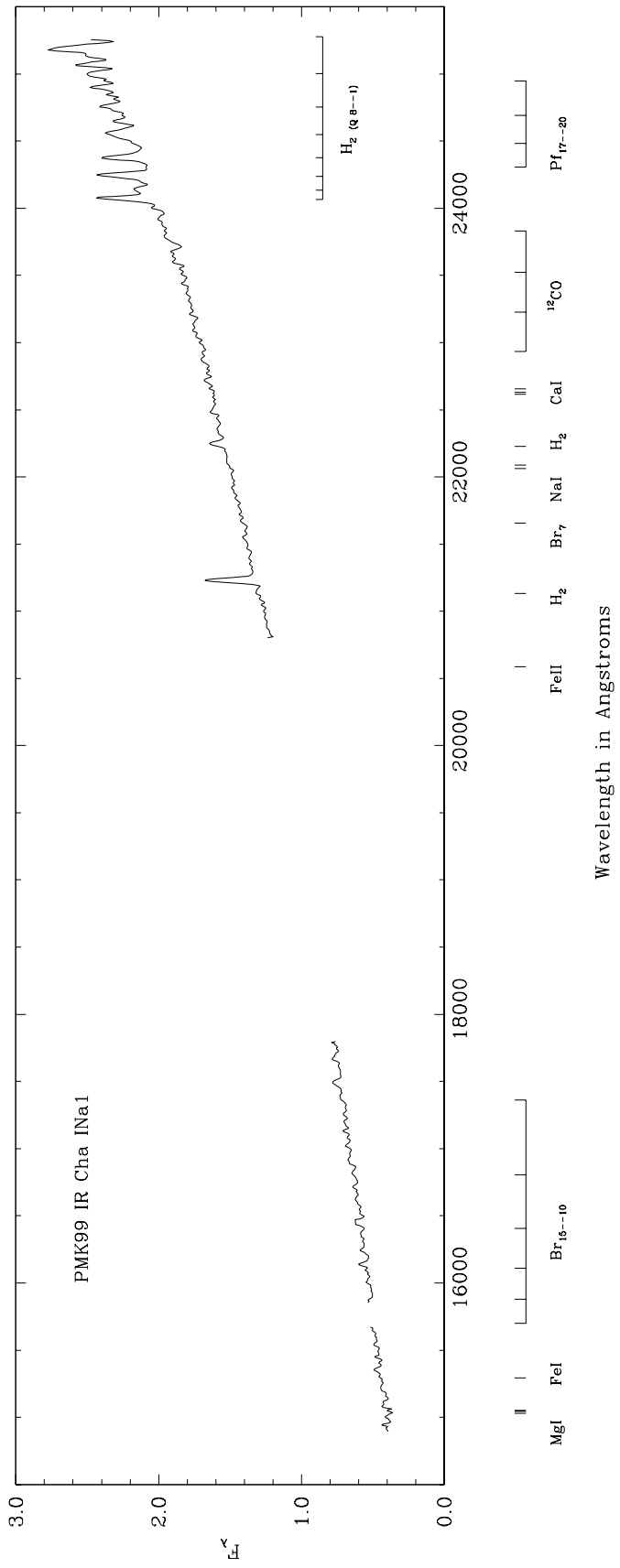

Fig. 5.— *HK* band spectrum of PMK99 IR Cha INa1. Molecular hydrogen lines, H_2 1-0 Q (1–8) and H_2 1-0 S (1–0), are in emission.

expressed by:

$$I_{H_2O} = (f1/f2)(f4/f3)^{0.76}. \quad (2)$$

The I_{H_2O} index allows us to derive spectral types for our candidate sources observed with both instruments as, in general, involves spectral regions of good S/N ratios.

We notice that the Q and I_{H_2O} indexes yield values which are independent of the extinction. They provide an appropriate tool to estimate spectral types for young stellar objects usually heavily obscured by the parent cloud dusty material.

Wilking et al. (1999) (**?**, see also)]cus00 obtained a linear relation to determine the M sub-type as function of Q using M dwarf standards with optically known spectral types (**?**, see equations (2) in)]wil99,cus00. These relations have been derived from standards whose spectra were telluric corrected using A0 V stars but whose continuum shapes were not restored (i.e., without multiplying by the Planck function spectrum at the temperature of the corresponding standard). As explained in Section 2 we used both G3-5 and O8 telluric standards for our SOFI data and thus our atmospheric telluric divided spectra (without correction for the slope of the standard spectrum) are not entirely comparable to those of Wilking et al. (1999) and Cushing et al. (2000). Nevertheless, Gómez & Persi (2002) noticed little dependence on the spectral type of the telluric standard in the analysis of ISOCAM sources of the Chamaeleon I dark cloud.

To check the applicability of these calibrations to our data we plot, in Figure 6, the optical spectral types vs the spectral types derived from the index Q for previously known objects. In this case we show the plot corresponding to the spectra telluric corrected using the O8 standards. The results are basically the same when we use the G5 stars. Our spectra of SZ 23 and GK-1 have relatively poor S/N ratio in the 2.4 – 2.5 μm region and the fluxes in the band F3 are very uncertain. These two objects were not included in Figure 6. We fit a linear relation to the data on this plot with a correlation coefficient r = 0.95. All spectral types derived from the index Q agree within 1.5 sub-type with the optical types. This difference is comparable to the accuracy expected by Wilking et al. (1999) and Cushing et al. (2000) for their calibrations.

We derive the index I_{H_2O} for previously known objects with optical spectral type observed with both instruments and obtain the following linear least-squares fit to the data:

$$M_{sub\_type} = (-14.22 \pm 1.25) + (15.07 \pm 1.08) \times I_{H_2O}, \quad (3)$$

with a correlation coefficient r = 0.94. We estimate a maximum uncertainty of about 1.7 subclasses in this calibration, considering *typical* errors in our measurements of the index I_{H_2O} and the correlation coefficient of equation 3. Gómez & Persi (2002) derived a similar relation of considerably lower precision based only on six previously known observed objects. We also determined equation (3) using only SOFI and OSIRIS data separately. Figure 7 shows

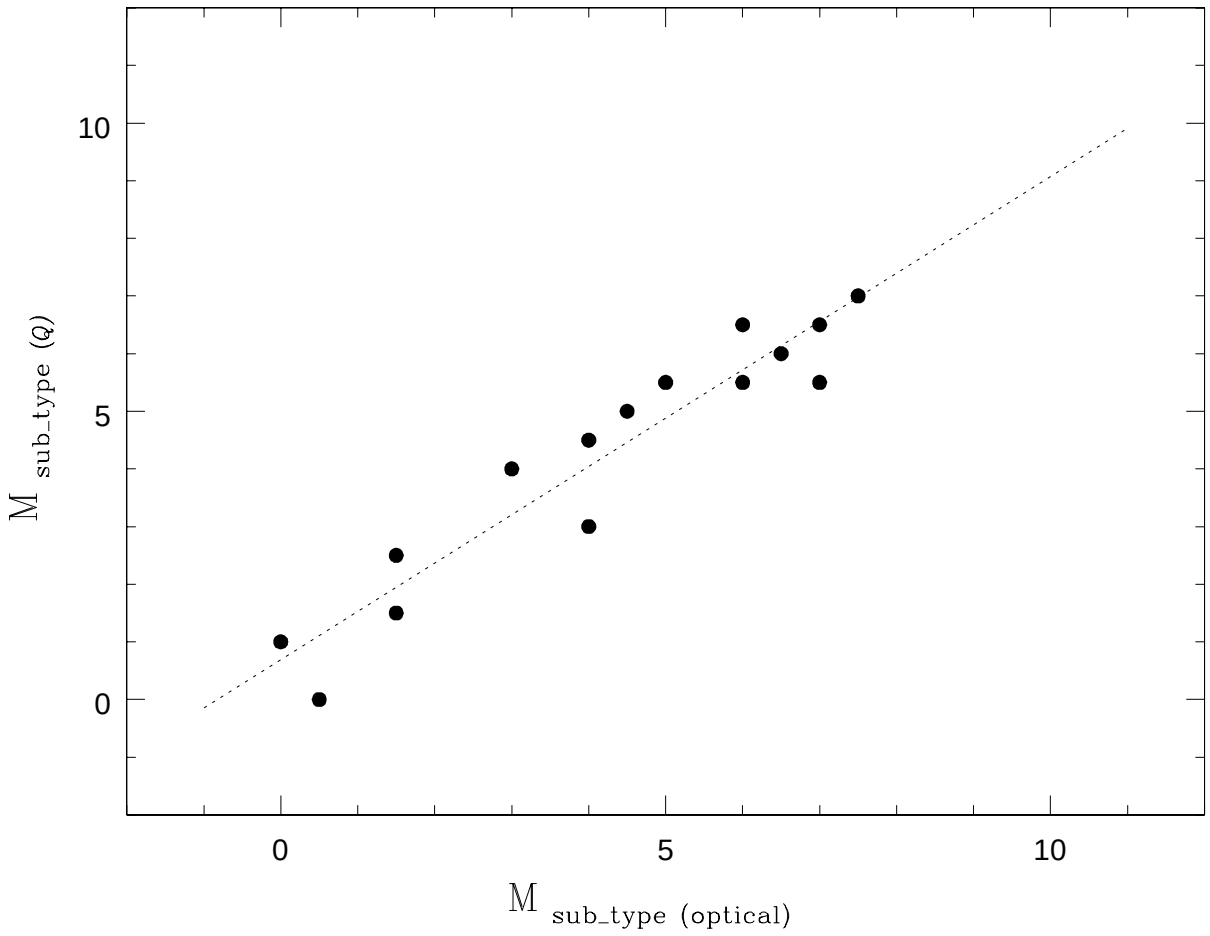

Fig. 6.— Optical $M_{sub-type}$ vs Q-index-derived $M_{sub-type}$ for previously known objects observed with SOFI. The dash line indicates a linear fit to the data.

the optical spectral types vs the spectral types derived from the index I_{H_2O} for previously known objects. Both calibrations agree within the 1.7 sub-classes uncertainty. Poor telluric corrections rendered unreliable the fluxes in one or more bands used by this index for several objects such as SZ 119, CHXR 78c, UY Cha, HO Lup, and SZ 77 and thus these stars were omitted in the derivation of equation 3.

In Table 7 we give spectral types derived from the application of these indexes for our candidate sources. Several objects in our sample such as CCE98 20, CCE98 35, CCE98 39, and CCE98 46 have very poor S/N spectra and thus spectral type derivations would be very uncertain. Other two near-infrared selected objects (CCE98 9 and GK2001 15) have better S/N spectra in relation to the ones mentioned above but still rather poor to attempt a reliable spectral type determination. Finally two objects with relatively good S/N spectra CCE98 40 and CCE98 44 have spectral types earlier than M0 justing from the significant Brγ equivalent width absorption lines (7 and 8 Å, respectively) and the absence of Na I, Ca I and CO features in their spectra (see Table 5).

Table 8 lists a group of previously known objects without optical spectral types in the literature for which we applied the water vapor indexes. Poor telluric corrections around 2.05 μm compromised the fluxes in the F3 and f3 bands (Q and I_{H_2O} indexes, respectively) and prevented us from obtaining spectral types for Ced 110 IRS 4 and Ced 110 IRS 6. HJM C 2-3 has a significant Brγ equivalent width ($\sim$ 12 Å) and no additional features indicative of a late spectral type. This object is probably earlier than M0.

For objects with SOFI spectra available we derive spectral type from both indexes and obtain a good agreement within 1.7 sub-class. However, it was not always possible to accurately measure the flux in the F3 band corresponding to the index Q due to poor S/N ratio in this spectral region. In these cases we adopted the spectral type given by the index I_{H_2O}.

To derive effective temperatures, intrinsic colors, and bolometric corrections for our targets from the estimated spectral types we adopted the corresponding calibrations obtained by Wilking et al. (1999). These relations comprise spectral types from M2 to M9. We supplemented these determinations with Kenyon & Hartmann (1995) relations in order to include M0-M1 stars.

3.5. Effects of veiling and surface gravity

The thermal emission from warm dust grains in circumstellar disks around young stellar objects may affect the observed water vapor bands and thus the spectral type estimates for our targets. This infrared excess emission can be characterized by $r_\lambda = F_\lambda^{exc}/F_\lambda^{phot}$, where F_λ^{exc} is the measured flux, including the excess (circumstellar) emission, and F_λ^{phot} is the flux due to the underlying stellar photosphere. Meyer et al. (1997) analyzed the near-infrared

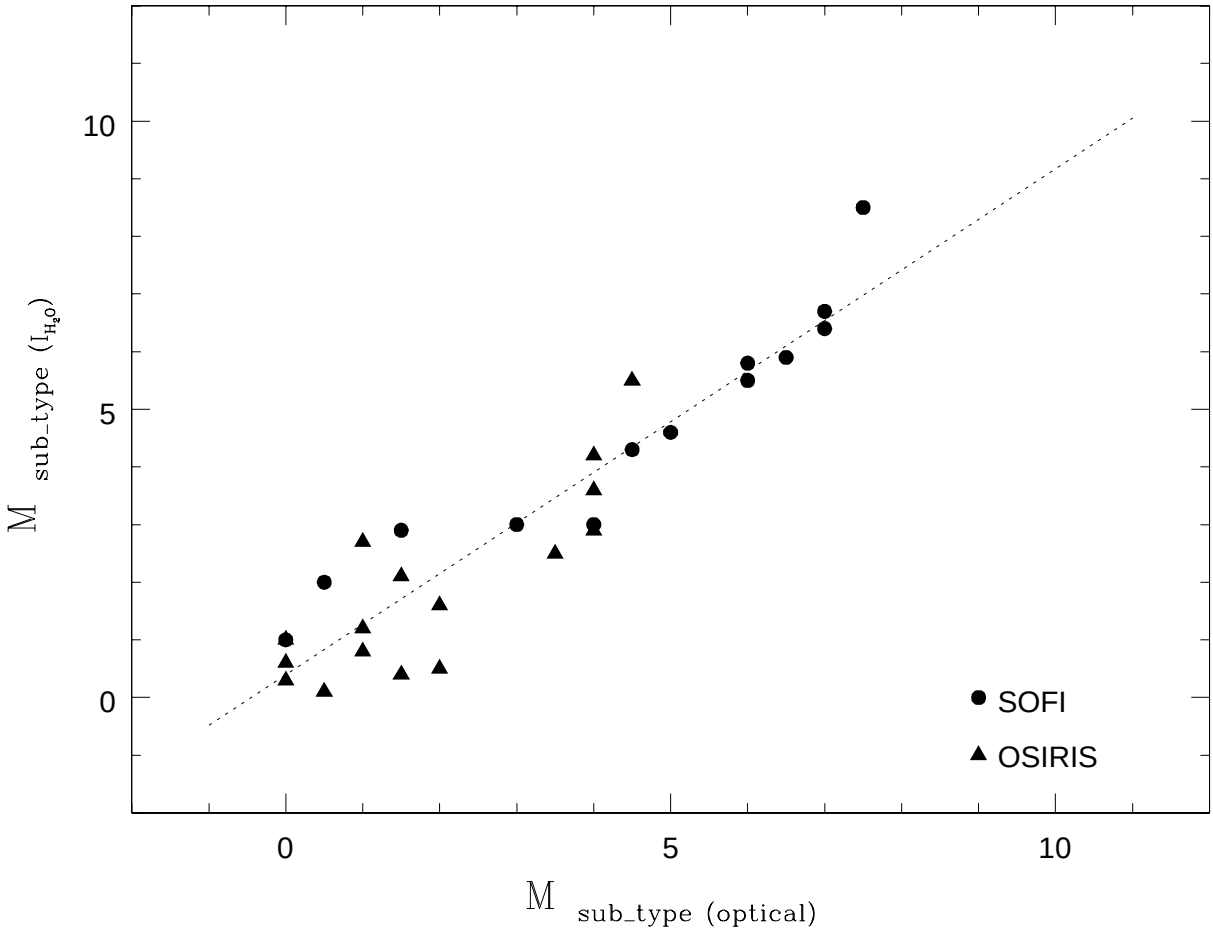

Fig. 7.— Optical $M_{sub-type}$ vs I_{H_2O}-index-derived $M_{sub-type}$ for previously known objects observed with SOFI and OSIRIS. The dash line indicates a linear fit to the data.

properties of T Tauri stars located in the Tarus-Auriga molecular cloud and derived median values of the J-, H-, and K-band excesses for the group of the CTTS and for the WTTS. They obtained $< r_J > = 0.0$, $< r_H > = 0.2$, and $< r_K > = 0.6$ for the CTTS and $< r_J > = < r_H > = < r_K > = 0.0$ for the WTTS. In Tables 7, 8, and 9 we give r_K, the K-band excess, estimated for our target objects using the following relation,

$$E(H-K) = (H-K) - (H-K)^{phot} - 0.077 \times A_V = -2.5 \times \log[1/(1+r_K)] \quad (4)$$

(**?**, see)]mey97. In this expression $(H-K)$ is the observed color (see Tables 3 and 4) and $(H-K)^{phot}$ corresponds to the intrinsic or photospheric color. The third term in equation (4) is related to the excess in color due only to the extinction to each individual target. To derive A_V we applied the Rieke & Lebofsky (1985) reddening law, $A_J = 0.28 A_V$, with

$$A_J = 2.63 \times E(J-H) \quad (5)$$

where, $E(J-H) = (J-H) - (J-H)_o$, is the color excess, and $(J-H)_o$, the intrinsic color.

Tables 7, 8, and 9 list A_J for the observed targets as well as the corresponding values of r_K. This estimate provides only a lower limit to the veiling as equation (4) assumes $r_H = r_J = 0$ (**?**, see)]mey97,wil99,cus00. However we expect the K-band excess, r_K, provides the main contribution to the total infrared excess, r_λ, in view of the median values for the CTTS in Taurus derived by Meyer et al. (1997).

Wilking et al. (1999) have simulated the spectra expected from young stars surrounded by circumstellar matter, adding the disk contribution to the spectra of known standard stars. These authors have then compared the index Q calculated for stars of known spectral types *with* and *without* the disk emission. The spectral types obtained from star+disk systems that have veiling effects of $r_K \sim 0.2$ are about 1 sub-class earlier than those derived for objects without the disk contribution. This effect increases as r_K increases and can account for $\sim$ 2-3 sub-classes earlier for $r_K \sim 0.6$.

Most objects in Tables 7, 8, and 9 have $r_K < 0.2$–0.3 with the exception of PMK99 IR Cha INa1 ($r_K = 0.7$). We expect our spectral type determinations using the water vapor indexes to be little affected by the effects of veiling except for PMK99 IR Cha INa1 that may actually have a spectral type $\sim$ 3 sub-types later than that given in Tables 7 according to its large K-band excess. It is also likely that in this case at least the H-band excess contribution be not negligible and then increases the total effect. In the Table 7 (in brackets) we adopt a minimum veiling correction of 3 sub-types later and indicate the corresponding derived parameters. We include this correction on the estimated mass and age for this object in section 3.6. We notice that any additional veiling correction would shift the object practically horizontally on the HR diagram corresponding to decreasing values of

mass and age. For example an additional increase of the spectral type in 0.5 sub-class (i.e., M7 spectral type) would give a mass of 0.05 M$\odot$ and an age of 2×10^5 yr for this object.

Pre-main sequence stars are known to have surface gravities intermediate between those of dwarfs (luminosity class V) and giants (luminosity class III) (**?**, e.g.,)]grme95, grla96. However we have determined spectral types for our targets neglecting this effect, in particular when applying the Q index versus the M spectral type relation derived by Wilking et al. (1999) and Cushing et al. (2000). These authors used M main sequence standards to obtain this calibration. To derive equation (3), the I_{H_2O} index calibration, we only used pre-main sequence stars with optically known spectral types and thus this relation may be more appropriate, in terms of the gravity effect, to obtain spectral types for our candidate young stellar objects.

Several authors (**?**, see, for example,)]wil99, cus00, gope02 have analyzed this effect on spectral type determinations and in general conclude that the surface gravity effect introduces a *typical* uncertainty of about 1–2 sub-classes. This estimate is appropriate for our water vapor index based spectral classification.

3.6. Luminosities, masses, and ages

We used the J magnitudes to estimate bolometric luminosities. This spectral band is less affected by contamination from circumstellar infrared excess emission than K or H. The bolometric luminosities are calculated from the following expressions:

$$\mathrm{Log}(\mathrm{L_{bol}}/\mathrm{L_\odot}) = 1.89 - 0.4 \times \mathrm{M_{bol}} \quad (6)$$

$$\mathrm{M_{bol}} = \mathrm{m_J} - \mathrm{A_J} - \mathrm{DM} + \mathrm{BC_J} \quad (7)$$

where, DM = 6.0 is the distance modulus and $\mathrm{BC_J}$ is the J band bolometric correction. $\mathrm{A_J}$[6] and $\mathrm{m_J}$ are the extinction and the apparent magnitude, respectively. Luminosities for the observed targets are given in Tables 7, 8, and 9. Our determinations agree within a factor of ~ 2 with previous derivations for the already known objects in the Chamaeleon I and Lupus clouds (**?**, cf.)]law96, com00, kra91, hug94.

We chose pre-main sequence evolutionary tracks and isocrones from D'Antona & Mazz-

[6]For a few objects with no H magnitude measurements we used the K band data in combination with the Rieke & Lebofsky (1985) reddening law ($\mathrm{A_J} = 1.66 \times \mathrm{E(J-K)}$, with $\mathrm{E(J-K)} = \mathrm{(J-K)} - \mathrm{(J-K)_o}$) to estimate the bolometric luminosities.

itelli (1994,1998)[7] to derive masses and ages for the observed sources. This model provides consistent and plausible results for our group of new targets, in reasonable agreement with the higher mass members of the cloud. In addition, D'Antona & Mazzitelli's (1994,1998) calculations include stars in a wide range of masses, from 3 M$\odot$ to objects well below the H burning limit (0.017 M$\odot$) and thus allows us an uniform and consistent derivation of masses and ages for our targets. Tables 7, 8, and 9 list these parameters. Figure 8 shows the location of new and previously known Chamaeleon I stars spectroscopically observed on the HR diagram.

We derived a mass of 0.19 M$\odot$ and an age of 4×10^6 yr for the source PMK99 IR Cha INa1 using the spectral type M3.5 given in Table 7. However as discussed in section 3.5 this object may actually have a spectral at least type 3 subtype later due to the high veiling ($r_K = 0.7$). To correct for the veiling effect we adopt a M6.5 spectral type and recalculate the corresponding bolometric luminosity ($Log(L_{bol}/L_\odot) = -1.36$). This shifts the star to the right practically horizontally on the HR diagram, corresponding to decreasing values of mass and age (0.06 M$\odot$ and 4×10^5 yr, respectively). In Table 7 we indicate in brackets the veiling corrected parameters. To our knowledge PMK99 IR Cha INa1 is the first substellar object associated with a bipolar outflow.

The candidate Chamaeleon I young stars (Figure 8) have masses between $\sim$ 0.7 and 0.04 M$\odot$. The previously known members of the cloud in Figure 8, roughly show the same range of masses and with the exception of LkHα 332-17 ($\sim$ 2.4 M$\odot$), one of the highest mass members of the cloud (**?**, see also)]law96. GK2001 18 with a mass of 0.04 M$\odot$ and PMK99 IR Cha INa1 with a mass of 0.06 M$\odot$ are the only two substellar objects detected among the observed Chamaeleon I candidates. The new objects have ages between $> 1 \times 10^5$ and $\sim 2 \times 10^7$ yr, roughly in agreement with the known members of the cloud (Lawson et al. 1996).

Our mass determinations for the known members agree within a factor of $\sim$ 2 with those derived by Lawson et al. (1996) and Comerón et al. (2000). We find that the age determinations agree within a *typical* factor of 4-5, except for HM 15, HM 16, Glass I and Cha Hα 1 – 6, for which we find a larger (about a factor of 10) difference in age. In the case Cha Hα 1 – 6 this difference is a least in part due to the use of different isocrones. Comerón et al. (2000) based their determination of ages on Burrows et al. (1997) and Baraffe et al. (1998) models whether we applied D'Antona & Mazzitelli's isocrones.

The Lupus previously known young stars span a range of ages of $\sim 3 \times 10^5$ and 1×10^6 yr and masses between $\sim$ 0.5 and 0.14 M$\odot$. The only exception is SZ 68, with a mass of 1.5 M$\odot$. Our determinations of mass and age agree within a factor of roughly 2 and 4, respectively with those derived by Hughes et al. (1994).

[7]Available at http://www.mporzio.astro.it/ dantona/prems.html.

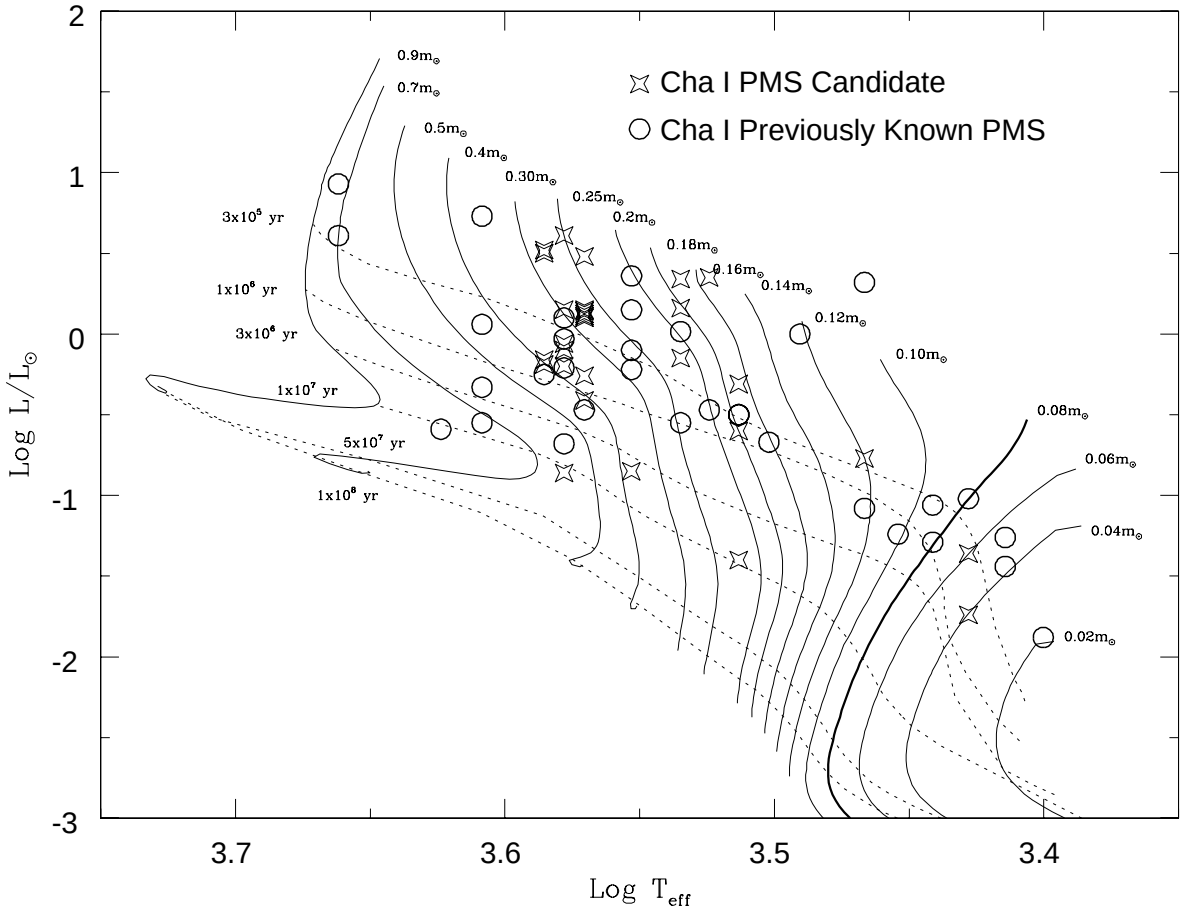

Fig. 8.— HR diagram showing the positions of the candidate and previously known pre-main sequence stars spectroscopically observed in the Chamaeleon I dark cloud. Pre-main sequence evolutionary tracks, indicated with continuous lines, are from D'Antona & Mazzitelli (1998). The thick continuous line corresponds to 0.08 M⊙, the H burning limit. The dashed lines correspond to the isocrones calculated also by the same authors.

3.7. Mass and age distributions

Lawson et al. (1996) derived the mass and age distributions for the Chamaeleon I dark cloud based on $\sim$ 80 previously known members of the cloud, adopting D'Antona & Mazzitelli's (1994) and Swenson et al. (1994) models. The mass distribution rises from $\sim$ 2 M$\odot$, peaks at 0.5-0.6 M$\odot$ and then falls towards lower masses. They obtained a median stellar mass of 0.55 M$\odot$ as representative of their sample. The age distribution peaks at ages $< 5 \times 10^6$ yr indicating a roughly constant rate of star formation during the last 5×10^6 yr and a rapidly declines towards older ages.

We combined our targets with those from Gauvin and Strom (1992), Lawson et al. (1996), Comerón et al. (2000) and Gómez & Persi (2002) to determine the mass and ages distribution for 145 objects belonging to the Chamaeleon I dark cloud. To analyze an homogeneous as possible data sample we estimated bolometric luminosities and effective temperatures for all the cloud members in the same manner as for the objects in Tables 7 and 8 (see Sections 3.4 and 3.5). We then used D'Antona & Mazzitelli's (1994,1998) evolutionary tracks and isocrones to derive masses and ages. Figure 9 indicates the mass and age distributions. The median mass is 0.30 M$\odot$. For the age distribution we obtained a median of 5×10^5 yr.

The mass histogram rises from about 2.5 M$\odot$ down to 0.4 M$\odot$, then falls off. We note a substantial decrease in the median mass of the stars in the Chamaeleon I dark cloud, from $\sim$ 0.55 M$\odot$ (Lawson et al. 1996) to about $\sim$ 0.30 M$\odot$. This is mainly due to the increasing number of mostly low mass and fainter members of the cloud detected by recent deep infrared survey of the cloud. The distribution of ages indicates an active star-formation episode within the last $\sim 5 \times 10^5$ yr and a decreasing rate at older ages (few $\times 10^7$ yr).

Comerón et al. (2000) intensively surveyed the central 300 arcmin^2 of the Chamaeleon I dark cloud, at different wavelengths combining both photometric and spectroscopic information. They detected 13 new members of the cloud and used Burrows et al. (1997) and Baraffe et al. (1998) models to identify 4 bona fide brown dwarfs, 6 transition (stellar/substellar) objects and 3 very low mass objects. In total this area contains 22 young stars with masses $<$ 1 M$\odot$. Assuming the pre-main sequence population in this region is essentially complete they measured the IMF and obtained a roughly flat behavior in logarithmic mass units within $\sim$ 1 and $\sim$ 0.03 M$\odot$. They also found that the majority of identified members in the region (19 out of 22) have ages near 2×10^6 yr and only 3 objects are significantly older, with ages of $\sim 2 \times 10^7$ yr.

The IMF of different star-forming regions (such as ρ Oph, Trapezium, IC 348, L1495E and Taurus) is approximately flat from the substellar regimen to $\sim$ 0.6–0.4 M$\odot$ (**?**, see)and the references therein]luh00. We interpret the fall off of the current IMF for the whole Chamaeleon I dark cloud as population selection effect. Assuming that the *true* shape of the function is roughly flat in logarithmic mass bins from the subsolar to the substellar regimen

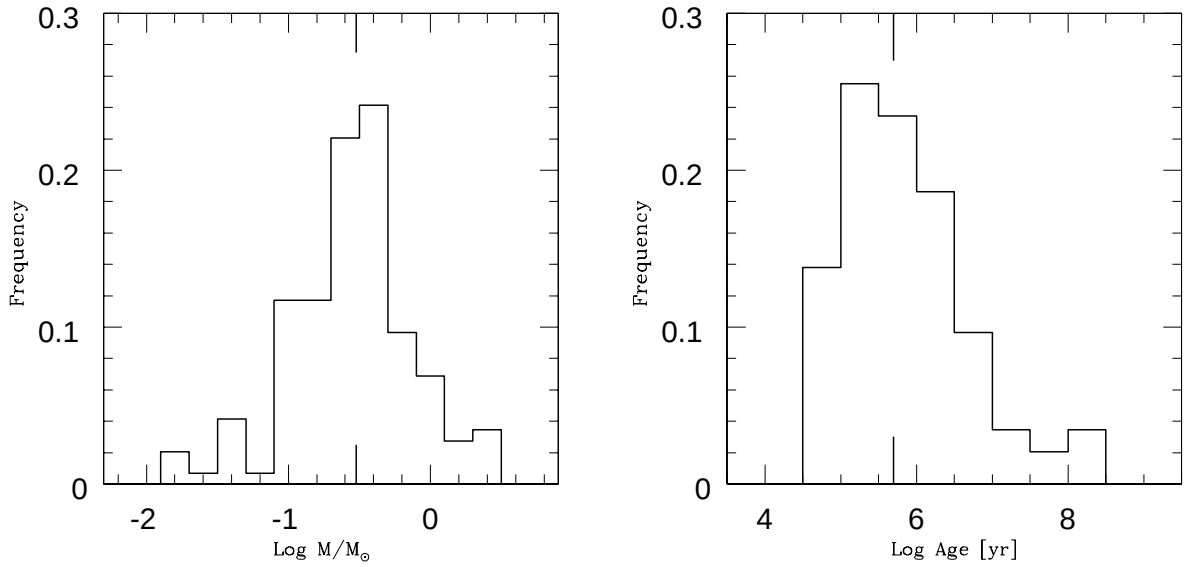

Fig. 9.— Mass and age distributions for the Chamaeleon I stars using the D'Antona & Mazzitelli evolutionary tracks and isocrones. The medians of each distributions are marked at the upper and lower axis. For the mass distribution we derive a median of 0.30 M⊙. The median age is 5×10^5 yr.

and that the census of young stars in the cloud for masses > 0.4 M$\odot$ is basically complete, we estimate that ~ 100 stars with masses between 0.4 and 0.04 M$\odot$ remain to be identified in the cloud.

4. Summary and Conclusions

We present near-infrared low resolution (R ~ 500) spectra of 46 candidate young stellar objects in the Chamaeleon I cloud with *typically* $K < 12$. We also observed 63 previously known young stellar objects belonging to this star-forming region and other southern hemisphere clouds. Both groups have similar spectroscopic characteristics. We used the water vapor indexes to derive spectral types for the new sources and adopted D'Antona & Mazzitelli (1998) evolutionary tracks and isocrones to estimate masses and ages. The majority of the new objects have masses between 0.7 and 0.15 M$\odot$; with only two sources with masses in the substellar regimen. One of these stars (PMK99 IR Cha INa1, with a mass of ~ 0.06 M$\odot$) is associated with the bipolar outflow detected by Mattila et al. (1989) in the northern part of the cloud. The other object, GK2001 18, has an estimated mass of 0.04 M$\odot$.

The mass distribution rises from about 2.5 M$\odot$, has a peak around 0.4 M$\odot$ and then falls towards lower masses. The median mass for the 145 compiled stars in the Chamaeleon I dark cloud is ~ 0.30 M$\odot$, representing a significant decrease with respect to the ~ 0.55 M$\odot$ derived by Lawson et al. (1996) from ~ 80 known members. The scarcity of very low mass objects is interpreted as an observational selection effect toward the fainter (and thus least massive) members of the cloud. We assume the *true* IMF of the whole cloud is roughly flat in logarithmic mass bins in the interval 0.4 – 0.04 M$\odot$ as found by Comerón et al. (2000) in the central 300 arcmin^2 region. If the current pre-main sequence population with masses > 0.4 M$\odot$ is complete, we estimate that ~ 100 stars with masses within these limits remain to be identified in the cloud. The age distribution indicates an active star-formation episode within the last $\sim 5 \times 10^5$ yr and a decreasing rate at older ages (few $\times 10^7$ yr).

The new 46 candidates analyzed in this paper are, on average, roughly 1.5 mag fainter in the K band than those included in Lawson et al. (1996) sample. These new objects include only two substellar objects; the rest of the stars have sub-solar masses down to $\sim$ 0.15 M$\odot$. However, ~ 150 fainter candidate members of the Chamaeleon I cloud (*typically* $K > 13$) remain to be spectroscopically characterized (Cambrésy et al. 1998; Persi et al. 1999; Oasa et al. 1999; Persi et al. 2000; Gómez & Kenyon 2001; Persi et al. 2001). These objects may contain at least part of the missing population within the interval 0.4 — 0.04 M$\odot$. Near-infrared spectra, in combination with pre-main sequence evolutionary tracks and isocrones, would be useful to determine the masses and ages of these objects. This information would provide a precise determination the behavior of the IMF, particular towards and into the substellar regimen for the whole cloud.

We thank Leonardo Vanzi (ESO) and Robert Blum (CTIO) for technical support with SOFI and OSIRIS, respectively. An anonymous referee provided useful suggestions that improved the content and presentation of this paper. This research has made use of the SIMBAD database, operated at CDS, Strasbourg, France. DM gratefully acknowledges support from Universidad de Chile FONDAP 15010003 and DID project I021-98/2.

REFERENCES

Alcalá, J. M., Krautter, J., Schmitt, J. H. M. M., Covino, E., Wichmann, R., & Mundt, R. 1995, A&AS, 114, 109

Appenzeller, I., Jankovics, I., & Krautter, J. 1983, A&AS, 53, 291

Baraffe, I., Chabrier, G., Allard, F., & Hauschildt, P. H. 1998, A&A, 337, 403

Baud B., Young E., Beichman C. A., Beintema D. A., Emerson J. P., Habing H. J., Harris S., Jennings R. E., Marsden P. L., & Wesselius P. R. 1984, ApJ, 278, 53

Bessell, M. S., & Brett, J. M. 1988, PASP, 100, 1134

Boulanger, F., Bronfman, L., Dame, T. M., & Thaddeus, P. 1998, A&A, 332, 273

Burrows, A., Marley, M., & Hubbard, W. B., et. al. 1997, ApJ, 491, 856

Burton, M. G., Brand, P. W. J. L., Geballe, T. R., & Webster, A. S. 1989, MNRAS, 236, 409

Cambrésy, L., Copet, E., Epchtein, N., de Batz, B., Borsenberger, J., Fouqué, P., Kimeswenger, S., & Tiphéne, D. 1998, A&A, 338, 977

Cohen, M., & Kuhi, L. V. 1979, ApJS, 41, 743

Comerón, F., Neuhäuser, R., & Kaas, A. A. 2000, A&A, 359, 269

Comerón, F., Rieke, G. H., & Neuhäuser, R. 1999, A&A, 343, 477

Covino, E., Alcalá, J. M., Allain, S., Bouvier, J., Terranegra, L., & Krautter, J. 1997, A&A, 328, 187

Cushing, M. C., Tokunaga, A. T., & Kobayashi, N. 2000, AJ, 119, 3019

Eislöffel, J., Smith, M. D., & Davis, C. J. 2000, A&A, 359, 1147

Gauvin, L. S., & Strom, K. M. 1992, ApJ, 385, 217

Gómez, M., & Kenyon, S. J. 2001, AJ, 121, 974

Gómez, M., & Persi, P. 2002, A&A, 389, 494

Greene, T. P., & Lada, C. J. 1996, AJ, 112, 2184

Greene, T. P., & Meyer, M. R. 1995, ApJ, 450, 233

Hartigan, P. 1993, AJ, 105, 1511

Hyland A. R., Jones T. J., & Mitchell R. M. 1982, MNRAS, 201, 1095

Hughes, J., Hartigan, P., Krautter, J., & Kelemen, J. 1994, AJ, 108, 1071

Kenyon, S. J., & Hartmann, L. 1995, ApJS, 101, 117

Kenyon, S. J., & Gómez, M. 2001, AJ, 121, 2673

Kleinmann. S. G., & Hall, D. N. B. 1986, ApJS, 62, 501

Krautter, J. 1991, in Low Mass Star Formation in Southern Molecular Clouds, edited by B. Reipurth, ESO Scientific Report No. 11, p. 127

Lawson, W. A., Feigelson, E. D., & Huenemoerder, D. P. 1996, MNRAS, 280, 1071

Lidman, C., Cuby, J-G., Vanzi, L., & Hainaut, O. 2000, SOFI User's Manual, Doc. No. LSO-MAN-ESO-40100-0003, Issue 1.3 (available at: http://www.ls.eso.org/lasilla/Telescopes/NEWNTT/sofi/manual/SOFImanual.html)

Luhman, K. L. 2000, ApJ, 544, 1044

Mattila, K., Lijeström, T., & Toriseva, M., 1989, in Low Mass Star Formation and Pre-Main Sequence Objects, edited B. Reipurth (Garching: ESO) p. 153

Meyer, M. R., Calvet, N., & Hillenbrand, L. A. 1997, AJ, 114, 288

Meyer, M. R., Edwards, S., Hinkle, K. H., & Strom, S. 1998, ApJ, 508, 397

Mizuno, A., Yamaguchi, R., Tachihara, K., Toyoda, S., Oayama, H., Yamamoto, H., Onishi, T., & Fukui, Y. 2001, PASJ, 53, 1071

Neuhäuser, R., & Comerón, F. 1999, A&A, 350, 612

Oasa, Y., Tamura, M., & Lawson, W. A. 1999, ApJ, 526, 336

Persi, P., Marenzi, A. R., Kaas, A. A., Olofsson, G., Nordh, L., & Roth, M. 1999, AJ, 117, 439

Persi, P., Marenzi, A. R., Gómez, M., & Olofsson, G. 2001, A&A, 376, 907

Persi, P., Marenzi, A. R., Olofsson, G., Kaas, A. A., Nordh, L., Huldtgren, M., Abergel, A., André, P., Bontemps, S., Boulanger, F., Burgdorf, M., Casali, M. M., Cesarsky, C. J., Copet, E., Davies, J., Falgarone, E., Montmerle, T., Perault, M., Prusti, T., Puget, J. L., & Sibille, F. 2000, A&A, 357, 219

Rieke, G. H., & Lebofsky, M. J. 1985, AJ, 288, 618

Rosenthal, D., Bertoldi, F., & Drapatz, S. 2000, A&A, 356, 705

Shevchenko, S. V., & Herbst, W. 1998, AJ, 116, 1419

Swenson, F. J., Faulkner, J., Rogers, F. J., & Iglesias, C. A. 1994, ApJ, 425, 286

Wallace, L., & Hinkle, K. 1997, ApJS, 111, 445

Wallace, L., Meyer, M. R., Hinkle, K., & Edwards, S. 2000, ApJ, 535, 325

Whittet, D. C. B., Prusti, T., Franco, G. A. P., Gerakines, P. A., Kilkenny, D., Larson, K., & Wesselius, P. R. 1997, A&A, 327, 1194

Wilking, B. A., Greene, T. P., & Meyer, M. R. 1999, AJ, 117, 469

Table 1. Candidate Chamaeleon I young stellar objects

Name	α(2000.0)	δ(2000.0)	Instrument	Date	Other ID.
CCE98 1	10 58 22.9	−78 29 49	OSIRIS	1999 May 08	
CCE98 2	10 59 12.3	−78 26 40	OSIRIS	1999 May 08	
CCE98 5	11 01 32.1	−77 42 10	OSIRIS	1999 May 07	
CCE98 8	11 02 47.1	−77 38 10	OSIRIS	1999 May 08	
CCE98 9	11 03 11.5	−77 36 36	OSIRIS	1999 May 08	ISO-ChaI 16
CCE98 12	11 04 11.2	−77 50 13	SOFI	1999 Apr 12	ISO-ChaI 40
GK2001 3	11 04 49.2	−78 04 46	OSIRIS	2002 Feb 28	
CCE98 14	11 05 19.2	−77 57 39	SOFI	1999 Apr 12	
CCE98 16	11 05 24.1	−76 07 44	OSIRIS	1999 May 07	
CCE98 17	11 05 54.4	−77 38 43	SOFI	1999 Apr 10	ISO-ChaI 69
CCE98 18	11 05 55.2	−77 35 13	SOFI	1999 Apr 12	ISO-ChaI 70
CCE98 19	11 06 15.9	−77 37 51	SOFI	1999 Apr 10/12	ISO-ChaI 76
CCE98 20	11 06 18.9	−77 35 18	SOFI	1999 Apr 12	
GK2001 15	11 07 06.5	−76 37 17	OSIRIS	2002 Feb 28	
CCE98 21	11 07 09.6	−77 18 47	SOFI	1999 Apr 12	ISO-ChaI 91
CCE98 23	11 07 16.5	−77 23 08	SOFI	1999 Apr 10/11	ISO-ChaI 97
CCE98 24	11 07 21.7	−77 22 12	SOFI	1999 Apr 10/11	BYB 35,ISO-ChaI 101
CCE98 25	11 07 23.7	−77 41 25	OSIRIS	1999 May 07	ISO-ChaI 102
CCE98 26	11 07 36.9	−77 35 19	SOFI	1999 Apr 11	ISO-ChaI 107
CCE98 27	11 07 37.5	−77 33 09	SOFI	1999 Apr 11	ISO-ChaI 109
GK2001 18	11 07 46.9	−76 15 17	OSIRIS	2002 Feb 28	
CCE98 32	11 08 04.2	−77 38 43	OSIRIS	1999 May 07	ISO-ChaI 126
CCE98 33	11 08 12.1	−77 18 54	SOFI	1999 Apr 11	ISO-ChaI 130
CCE98 34	11 08 12.9	−77 19 13	SOFI	1999 Apr 11	ISO-ChaI 131
GK2001 21	11 08 22.6	−76 49 19	OSIRIS	2002 Feb 28	
GK2001 24	11 08 44.5	−76 13 29	OSIRIS	2002 Feb 28	
CCE98 35	11 08 57.2	−77 43 28	SOFI	1999 Apr 10	
ISO-ChaI 177	11 09 08.5	−76 49 13	OSIRIS	2002 Feb 27	
CCE98 36	11 09 11.4	−76 32 50	SOFI	1999 Apr 12	OTS99 2
CCE98 37	11 09 12.0	−77 39 06	OSIRIS	1999 May 07	ISO-ChaI 179
CCE98 39	11 09 23.3	−76 31 14	SOFI	1999 Apr 12	
CCE98 40	11 09 26.9	−76 33 33	SOFI	1999 Apr 12	OTS99 13,HJM C 1-3
PMK99 IR Cha INa1	11 09 29.4	−76 33 28	SOFI	1999 Apr 10/12	ISO-ChaI 192,CCE98 41,OTS99 15
PMK99 IR Cha INa2	11 09 36.6	−76 33 39	SOFI	1999 Apr 10	OTS99 18
CCE98 42	11 09 38.0	−77 10 41	OSIRIS	1999 May 07	ISO-ChaI 196
CCE98 43	11 09 43.5	−76 33 31	SOFI	1999 Apr 10	HJM C 1-21,OTS99 21
CCE98 44	11 09 47.7	−76 34 06	SOFI	1999 Apr 10	HJM C 1-22,OTS99 25
CCE98 46	11 09 53.4	−77 17 16	SOFI	1999 Apr 11	
CCE98 47	11 09 56.7	−77 18 26	SOFI	1999 Apr 11	ISO-ChaI 227
PMK99 IR Cha INa3	11 10 01.5	−76 32 50	SOFI	1999 Apr 10	OTS99 30
PMK99 IR Cha INa4	11 10 04.5	−76 33 09	SOFI	1999 Apr 10	OTS99 32
CCE98 48	11 10 11.9	−76 35 31	SOFI	1999 Apr 11	ISO-ChaI 237,HJM C 1-8,OTS99 45
CCE98 49	11 10 54.0	−77 25 03	SOFI	1999 Apr 11	ISO-ChaI 256
GK2001 42	11 11 21.1	−78 05 20	OSIRIS	2002 Feb 28	
CCE98 50	11 11 29.5	−76 09 29	OSIRIS	1999 May 07	
CCE98 51	11 11 32.4	−77 28 12	OSIRIS	1999 May 07	

References. — BYB: Baud et al. (1984), CCE98: Cambrésy et al. (1998), GK2001: Gómez & Kenyon (2001), HJM C: Hyland et al. (1982), OTS99: Oasa et al. (1999), ISOCAM Cha INa: Persi et al. (1999), ISO-ChaI: Persi et al. (2000).

Table 2. Previously known young stellar objects observed

Name	α(2000.0)	δ(2000.0)	Instrument	Date
Chamaeleon I				
Hn 1	11 02 33.1	−77 29 26	OSIRIS	1999 May 08
BYB 18	11 04 43.0	−77 41 57	OSIRIS	1999 May 06
CHXR 73	11 06 26.5	−77 37 38	SOFI	1999 April 10
Ced 110 IRS 4	11 06 48.1	−77 22 29	SOFI	1999 Apr 11
CHXR 74	11 06 54.0	−77 42 09	SOFI	1999 Apr 10
UY Cha	11 06 59.5	−77 18 54	SOFI	1999 Apr 12
Ced 110 IRS 6	11 07 10.5	−77 23 10	SOFI	1999 Apr 11
Hn 6	11 07 13.0	−77 46 39	OSIRIS	1999 May 08
Cha Hα 1	11 07 16	−77 35 54	SOFI	1999 Apr 10
LkHα 332-17	11 07 20.7	−77 38 07	OSIRIS	1999 May 06
BYB 34	11 07 35.3	−77 34 05	SOFI	1999 Apr 10
CHXR 26	11 07 37.0	−77 33 33	OSIRIS	1999 May 06
Cha Hα 2	11 07 42.7	−77 34 00	SOFI	1999 Apr 10
HM 15	11 07 44.5	−77 39 43	SOFI	1999 Apr 10
Cha Hα 3	11 07 58.2	−77 37 21	SOFI	1999 Apr 10
SZ 23	11 07 58.4	−77 42 42	SOFI	1999 Apr 10
HM 16	11 07 59.1	−77 38 46	SOFI	1999 Apr 10
VW Cha	11 08 01.8	−77 42 29	SOFI/OSIRIS	1999 Apr 10/1999 May 06
Glass I	11 08 15.4	−77 33 53	OSIRIS	1999 May 06
HM 19	11 08 16.9	−77 44 37	OSIRIS	1999 May 06
Cha Hα 4	11 08 20.6	−77 39 19	SOFI	1999 Apr 10
Cha Hα 5	11 08 24.7	−77 41 47	SOFI	1999 Apr 10
Cha IR Nebula	11 08 38.7	−77 43 51	SOFI	1999 Apr 10
Cha Hα 6	11 08 39.6	−77 34 17	SOFI	1999 Apr 10
CHXR 78c	11 08 54.2	−77 32 12	OSIRIS	1999 May 06
HJM C 1-6	11 09 23.5	−76 34 32	SOFI	1999 Apr 12
HJM C 7-2	11 09 25.9	−77 26 25	SOFI	1999 Apr 12
HJM C 1-25	11 09 41.8	−76 34 59	SOFI	1999 Apr 11
HJM C 2-3	11 09 46.8	−76 43 54	SOFI	1999 Apr 12
Hn 10	11 09 47.5	−76 34 45	SOFI	1999 Apr 11
BYB 43	11 09 47.9	−77 26 30	SOFI	1999 Apr 12
HJM C 1-2	11 09 55.0	−76 32 40	SOFI	1999 Apr 11
HJM C 7-3	11 10 00.0	−77 26 33	SOFI	1999 Apr 12
Hn 11	11 10 04.9	−76 33 28	SOFI	1999 Apr 11
GK-1	11 10 04.9	−76 35 47	SOFI	1999 Apr 11
BYB 53	11 14 50.8	−77 33 39	OSIRIS	1999 May 07
Lupus				
SZ 65	15 39 27.7	−34 46 17	OSIRIS	1999 May 09
SZ 68	15 45 12.9	−34 17 31	OSIRIS	1999 May 06
SZ 77	15 51 47	−35 56 43	OSIRIS	1999 May 08
SZ 82	15 56 09.3	−37 56 06	OSIRIS	1999 May 08
SZ 128	15 58 07.4	−41 51 48	SOFI	1999 Apr 10
HO Lup	16 07 00.6	−39 02 19	OSIRIS	1999 May 09
SZ 90	16 07 10.1	−39 11 03	OSIRIS	1999 May 07
SZ 94	16 07 49.6	−39 04 29	SOFI	1999 Apr 12
SZ 96	16 08 12.6	−39 08 33	OSIRIS	1999 May 06
HK Lup	16 08 22.5	−39 04 46	OSIRIS	1999 May 06
SZ 103	16 08 30.3	−39 06 11	OSIRIS	1999 May 09

Table 2—Continued

Name	α(2000.0)	δ(2000.0)	Instrument	Date
Eggen 2	16 08 42.7	−39 06 18	OSIRIS	1999 May 06
SZ 114	16 09 01.8	−39 05 12	OSIRIS	1999 May 08
SZ 117	16 09 44.3	−39 13 30	OSIRIS	1999 May 08
SZ 123	16 10 51.5	−38 53 14	OSIRIS	1999 May 08
SZ 119	16 09 57.1	−38 59 48	SOFI/OSIRIS	1999 Apr 10/1999 May 07
SZ 121	16 10 12.2	−39 21 01	SOFI	1999 Apr 10
SZ 122	16 10 16.4	−39 08 00	OSIRIS	1999 May 06
SZ 124	16 11 53.3	−39 02 16	SOFI/OSIRIS	1999 Apr 10/1999 May 08
Other clouds				
RX J0842.4-8345	08 42 22.4	−83 45 24	SOFI	1999 Apr 11
RX J0844.8-7846	08 44 50.8	−78 46 55	SOFI	1999 Apr 11
RX J0915.5-7608	09 15 30	−76 08 00	SOFI	1999 Apr 11
RX J0951.9-7901	09 51 50.7	−79 01 38	SOFI	1999 Apr 11
Haro 1-1	16 21 34.4	−26 12 25	OSIRIS	1999 May 08
ROX 13	16 26 29	−24 19 42	OSIRIS	1999 May 07
Lkhα 104	18 02 54.3	−24 20 56	OSIRIS	1999 May 07
RNO 93	17 16 13.8	−20 57 46	OSIRIS	1999 May 07

Table 3. Compiled photometry for the Chamaeleon I candidate young stellar objects

Name	I	J	H	K	Reference
CCE98 1	11.09	9.08	···	7.50	(1)
CCE98 2	10.65	8.93	···	7.47	(1)
CCE98 5	13.57	10.73	···	8.68	(1)
CCE98 8	···	13.75	···	10.50	(1)
CCE98 9	···	13.40	···	10.01	(1)
CCE98 12	18.48	13.77	11.52	10.55	(1), (2)
GK2001 3	···	14.26	13.23	12.48	(2)
CCE98 14	18.13	13.65	11.46	10.57	(1), (2)
CCE98 16	11.99	10.00	···	8.41	(1)
CCE98 17	15.52	11.46	9.77	9.04	(1), (2)
CCE98 18	17.98	13.32	10.96	9.92	(1), (2)
CCE98 19	16.55	12.59	10.93	10.26	(1), (2)
CCE98 20	···	16.47	14.19	13.22	(1)
GK2001 15	···	12.65	11.72	10.22	(2)
CCE98 21	···	14.66	12.46	11.27	(2)
CCE98 23	···	17.55	13.60	10.97	(2)
CCE98 24	···	15.20	12.42	10.83	(2)
CCE98 25	12.32	9.46	8.09	7.63	(1), (2)
CCE98 26	16.31	12.44	10.75	9.91	(1), (2)
CCE98 27	18.03	13.60	11.73	10.91	(1), (2)
GK2001 18	···	13.87	12.93	12.22	(2)
CCE98 32	14.39	11.51	9.67	8.30	(1), (2)
CCE98 33	···	14.28	11.72	10.47	(2)
CCE98 34	···	12.79	10.28	8.90	(2)
GK2001 21	···	14.26	13.44	12.32	(2)
GK2001 24	···	14.27	13.71	12.92	(2)
CCE98 35	···	15.52	13.86	12.56	(2)
ISO-ChaI 177	···	13.02	12.20	11.56	(2)
CCE98 36	···	14.42	···	11.68	(1)
CCE98 37	16.14	12.86	11.17	10.47	(1), (2)
CCE98 39	18.20	14.36	12.62	11.82	(1), (2)
CCE98 40	17.77	13.15	11.19	10.17	(1), (2)
PMK99 IR Cha INa1	···	18.24	15.28	12.75	(3)
PMK99 IR Cha INa2	···	18.25	16.72	15.97	(4)
CCE98 42	15.28	11.43	9.81	9.11	(1), (2)
CCE98 43	···	15.56	13.26	12.29	(2)
CCE98 44	···	15.36	13.09	11.86	(2)
CCE98 46	···	15.66	13.38	12.42	(2)
CCE98 47	16.58	12.36	10.62	9.86	(1), (2)
PMK99 IR Cha INa3	···	17.79	16.31	14.98	(3)
PMK99 IR Cha INa4	···	17.47	15.92	14.36	(3)
CCE98 48	13.90	10.75	9.34	8.55	(1), (2)
CCE98 49	17.51	13.33	11.71	10.83	(1), (2)
GK2001 42	···	14.58	13.94	13.25	(2)
CCE98 50	12.78	9.88	···	7.99	(1), (2)
CCE98 51	14.90	11.72	10.17	9.61	(1), (2)

References. — (1): Cambrésy et al. (1998), (2): Gómez & Kenyon (2001), (3): Persi et al. (1999), (4): Oasa et al. (1999).

Table 4. Previously known young stellar objects: Compiled photometry and optical spectral types

Name	I	J	H	K	Type[a]	ST	Referece
Chamaeleon I							
Hn 1	12.97	11.32	10.40	10.08	W	M2	(1), (2), (13)
BYB 18	13.63	11.80	11.01	10.64	W	···	(1), (2), (3)
CHXR 73	···	12.60	11.24	10.70	W	K3-M2	(2), (3)
Ced 110 IRS 4	···	16.53	13.88	12.57	···	···	(3)
CHXR 74	···	11.55	10.55	10.25	···	K7	(2),(3),(4)
UY Cha	12.92	11.10	10.33	9.91	C	M1.5	(1),(3),(5)
Ced 110 IRS 6	···	···	14.61	10.81	···	···	(3)
Hn 6	13.34	11.11	10.07	9.72	W	K7	(1), (2), (3), (13)
Cha Hα 1	16.4	13.42	12.76	12.31	C	M7.5	(3), (6)
LkHα 332-17	9.31	7.99	7.21	6.77	C	G2	(1), (3), (5)
BYB 34	14.43	12.19	11.30	10.95	W	M5	(1), (2), (3), (4)
CHXR 26	15.16	11.41	9.88	9.21	···	K7	(1), (2), (3)
Cha Hα 2	15.3	12.21	11.22	10.65	C	M6.5	(3), (6)
HM 15	12.56	10.22	9.05	8.42	C	M0.5	(1), (3), (5)
Cha Hα 3	15.0	12.35	11.69	11.27	W	M7	(3), (6)
SZ 23	14.58	11.85	10.62	9.81	C	M2.5	(1), (3), (4)
HM 16	12.76	9.71	8.19	7.16	C	K7	(1), (3), (4), (5)
VW Cha	10.56	8.63	7.72	7.17	C	K2-K5	(1), (3), (5), (14)
Glass I	10.54	8.58	7.40	6.22	W	K4	(1), (3), (5)
HM 19	13.04	11.29	10.41	10.12	W	M3.5	(1), (3)
Cha Hα 4	14.4	12.13	11.43	11.08	W	M6	(3), (6)
Cha Hα 5	14.7	12.13	11.21	10.78	W	M6	(3), (6)
Cha IR Nebula	15.86	11.12	9.30	8.07	···	···	(1), (3)
Cha Hα 6	15.1	12.37	11.53	11.04	C	M7	(3), (6)
CHXR 78c	14.75	12.36	11.54	11.17	W	M5.5	(1), (2), (3), (4)
HJM C 1-6	17.99	12.36	10.13	8.52	···	···	(1), (3)
HJM C 7-2	···	11.64	10.05	9.34	···	···	(7)
HJM C 1-25	···	13.48	11.15	9.63	···	···	(3)
HJM C 2-3	14.50	11.73	10.72	10.14	···	···	(1), (3)
Hn 10	14.81	11.94	10.68	9.96	···	···	(1), (3), (13)
BYB 43	16.02	12.61	11.12	10.12	···	···	(1), (3)
HJM C 1-2	···	13.42	10.98	9.25	···	···	(3)
HJM C 7-3	···	12.11	10.51	9.92	···	···	(7)
Hn 11	14.46	11.53	10.05	9.20	C	···	(1), (3), (13)
GK-1	12.86	10.39	9.48	9.10	W	M0	(3), (5), (14)
BYB 53	11.89	10.49	9.76	9.53	W	M1	(1), (2), (3)
Lupus							
SZ 65	10.51	9.19	8.39	7.99	C	M0-M0.5	(8), (14)
SZ 68	8.86	7.65	6.94	6.55	W	K2	(8)
SZ 77	10.83	9.53	8.72	8.34	C	M0	(8), (14)
SZ 82	10.20	8.87	8.10	7.75	W	M0	(8), (14)
SZ 128	12.70	11.19	10.29	9.71	W	M1.5	(8)
HO Lup	11.42	10.04	9.14	8.60	C	M1	(8)
SZ 90	13.28	10.46	9.44	8.82	C	K7-M0	(8), (14)
SZ 94	12.90	11.50	10.89	10.63	W	M4	(8)
SZ 96	11.84	10.21	9.35	8.90	C	M1.5	(8), (14)
HK Lup	10.92	9.55	8.64	7.99	C	K7-M0	(8), (14)
SZ 103	13.37	11.78	10.90	10.34	C	M4	(8), (14)

Table 4—Continued

Name	I	J	H	K	Type[a]	ST	Referece
Eggen 2	11.16	9.72	8.98	8.75	W	M1	(8)
SZ 114	12.12	10.42	9.62	9.18	C	M4	(8)
SZ 117	12.27	11.02	10.11	9.66	C	M2	(8)
SZ 123	12.78	11.20	10.36	9.91	C	M1	(8)
SZ 119	11.96	10.36	9.68	9.45	W	M4	(8)
SZ 121	11.84	10.27	9.49	9.13	W	M3	(8)
SZ 122	12.12	11.03	10.31	10.07	W	M2	(8)
SZ 124	11.46	10.38	9.79	9.48	W	K7-M0	(8)
Other clouds							
RX J0842.4-8345	10.53	9.44	8.82	8.65	W	K4-K6	(9), (10)
RX J0844.8-7846	10.70	9.61	8.93	8.72	W	K6-M0	(9), (10)
RX J0915.5-7608	10.35	9.37	8.71	8.52	W	K6-K7	(9), (10)
RX J0951.9-7901	9.29	8.66	8.20	8.09	W	G7-G8	(9), (10)
Haro 1-1	...	...	...	...	C	K5-K7	(11)
ROX 13	...	...	...	...	...	...	
Lkhα 104	...	...	...	...	C	K5	(12)
RNO 93	...	...	...	...	C	K5	(12)

[a]C and W refer to the classical and weak emission T Tauri type, (CTTS and WTTS)

References. — (1): Cambrésy et al. (1998), (2): Lawson et al. (1996), (3): Gómez & Kenyon (2001), (4): Comerón et al. (1999), (5): Gauvin and Strom (1992), (6): Neuhäuser & Comerón (1998), (7): Kenyon & Gómez (2001), (8): Hughes et al. (1994), (9): Alcalá et al. (1995), (10): Covino et al. (1997), (11): Shevchenko & Herbst (1998), (12): Cohen & Kuhi (1979), (13): Hartigan (1993) (14): Appenzeller et al. (1983).

Table 5. Equivalent widths (in Å) for the candidate young stars

Name [a]	Paβ	Brγ	Na I[b]	Ca I[c]	CO[d]
CCE98 1	···	2	6	4	46
CCE98 2	···	···	2	3	35
CCE98 5	···	2	3	···	28
CCE98 8	···	2	3	2	18
CCE98 9	···	···	3	···	8
CCE98 12	···	1	6	4	34
CCE98 14	···	···	3	3	28
CCE98 16	···	2	4	3	39
CCE98 17	···	2	···	1	15
CCE98 18	···	2	2	2	22
CCE98 19	···	···	5	5	20
CCE98 21	···	1	4	5	19
CCE98 23	···	···	3	3	11
CCE98 24	−8	−4	3	4	12
CCE98 25	···	3	6	···	65
CCE98 32	···	···	5	···	···
CCE98 33	···	2	1	1	24
CCE98 34	···	···	4	2	23
CCE98 36	···	1	···	···	19
CCE98 37	···	···	5	···	26
CCE98 40	···	7	···	···	···
PMK99 IR Cha INa1	···	···	···	···	···
CCE98 42	···	···	7	3	23
CCE98 43	···	···	4	···	21
CCE98 44	···	8	···	···	···
CCE98 47	···	2	···	···	17
CCE98 48	···	···	3	3	15
CCE98 50	···	···	5	2	35
CCE98 51	···	2	3	···	···

[a]Sources GK2001 3, CCE98 20, GK2001 15, GM 1, CCE98 26, CCE98 27, GK2001 18, GK2001 21, GK2001 24, CCE98 35, ISO-ChaI 177, CCE98 39, PMK99 IR Cha INa2, CCE98 46, PMK99 IR Cha INa3, PMK99 IR Cha INa4, CCE98 49, and GK2001 42 were not measured due to poor S/N on the corresponding spectrum.

[b]Na I doublet (2.206 and 2.209 μm)

[c]Ca I triplet (2.261, 2,263, and 2.266 μm)

[d]CO ν = 2-0, 3-1

Note. — Positive values indicate absorptions and negative values correspond to emissions. Missing equivalent widths indicate that the corresponding feature was not detected either in absorption or emission, at the resolution used and given the the S/N ratio for each spectrum.

Note. — For the SOFI data we estimate an uncertainty of $\sim$ 1-2 Å in the Paβ, Brγ, Na I doublet (2.206 and 2.209 μm), and Ca I triplet (2.261, 2,263, and 2.266 μm) equivalent widths. The combined CO ν = 2-0 and 3-1 bands have a slightly worse precision of $\sim$ 3 Å.

Note. — For the OSIRIS data we estimate an error of 2-3 Å in our measurements of Paβ, Brγ, Na I doublet, and Ca I triplet. The combined CO ν = 2-0, and 3-1 bands have a precision of $\sim$ 4-5 Å.

Table 6. Equivalent widths (in Å) for the observed previously known pre-main sequence stars

Name	Paβ	Brγ	Na I[a]	Ca I[b]	CO[c]	Note
Chamaeleon I						
Hn 1	···	···	3	2	8	
BYB 18	···	···	7	4	33	
CHXR 73	···	2	···	···	16	
Ced 110 IRS 4	···	···	···	···	···	
CHXR 74	···	···	6	5	13	
UY Cha	−5	−2	4	4	15	
Ced 110 IRS 6	···	−7	···	···	···	
Hn 6	···	···	5	4	10	
Cha Hα 1	···	···	···	···	13	
LkHα 332-17	−5	···	···	···	···	
BYB 34	···	···	5	6	12	
CHXR 26	···	···	9	···	···	
Cha Hα 2	···	···	5	6	12	
HM 15	−5	···	4	2	8	
Cha Hα 3	···	···	3	2	14	
SZ 23	−6	−2	6	5	9	
HM 16	−8	···	···	···	···	
VW Cha	−8	−3	4	2	7	SOFI data
VW Cha	−6	−2	5	···	6	OSIRIS data
Glass I	···	···	···	···	···	
HM 19	···	···	5	2	21	
Cha Hα 4	···	···	3	2	13	
Cha Hα 5	···	···	4	2	13	
Cha IR Nebula	···	···	2	2	16	
Cha Hα 6	···	···	3	2	10	
CHXR 78c	···	3	3	···	···	
HJM C 1-6	−10	−2	1	2	···	
HJM C 7-2	···	2	1	1	16	
HJM C 1-25	···	···	3	3	7	
HJM C 2-3	14	12	···	···	···	
Hn 10	−3	3	4	4	9	
BYB 43	−17	−4	3	2	9	
HJM C 1-2	···	···	2	2	5	
HJM C 7-3	···	2	3	2	19	
Hn 11	−9	−4	1	3	7	
GK-1	−2	1	6	4	23	
BYB 53	···	2	3	3	8	
Lupus						
SZ 65	···	···	2	···	6	
SZ 68	···	2	5	3	16	
SZ 77	···	2	2	3	11	
SZ 82	···	···	3	2	4	
SZ 128	−2	···	5	5	12	
HO Lup	−12	−2	···	···	4	
SZ 90	−8	···	···	2	···	
SZ 94	···	−6	10	4	17	
SZ 96	−2	···	3	···	1	
HK Lup	···	···	3	···	7	

Table 6—Continued

Name	Paβ	Brγ	Na I[a]	Ca I[b]	CO[c]	Note
SZ 103	···	3	4	7	19	
Eggen 2	···	4	4	6	···	
SZ 114	···	···	4	···	3	
SZ 117	···	···	3	···	3	
SZ 123	−8	···	2	3	2	
SZ 119	···	···	6	4	15	SOFI data
SZ 119	···	···	4	7	13	OSIRIS data
SZ 121	···	···	6	6	15	
SZ 122	···	···	4	5	5	
SZ 124	···	···	6	6	12	SOFI data
SZ 124	···	···	5	6	8	OSIRIS data
Other clouds						
RX J0842.4-8345	···	···	6	5	8	
RX J0844.8-7846	···	···	5	5	11	
RX J0915.5-7608	···	···	5	5	11	
RX J0951.9-7901	···	···	3	3	5	
Haro 1-1	−16	−11	2	2	···	
ROX 13	···	2	5	6	11	
Lkhα 104	···	2	···	···	···	
RNO 93	···	···	4	3	11	

[b]Na I doublet (2.206 and 2.209 μm)

[c]Ca I triplet (2.261, 2,263, and 2.266 μm)

[d]CO ν = 2-0, 3-1

Note. — Positive values indicate absorptions and negative values correspond to emissions. Missing equivalent widths indicate that the corresponding feature was not detected either in absorption or emission, at the resolution used and given the the S/N ratio for each spectrum.

Note. — For the SOFI data we estimate an uncertainty of $\sim$ 1-2 Å in the Paβ, Brγ, Na I doublet (2.206 and 2.209 μm), and Ca I triplet (2.261, 2,263, and 2.266 μm) equivalent widths. The combined CO ν = 2-0 and 3-1 bands have a slightly worse precision of $\sim$ 3 Å.

Note. — For the OSIRIS data we estimate an error of 2-3 Å in our measurements of Paβ, Brγ, Na I doublet, and Ca I triplet. The combined CO ν = 2-0, and 3-1 bands have a precision of $\sim$ 4-5 Å.

Table 7. Spectral types and derived parameters for the Chamaeleon I candidate young stellar objects

Name	Q^a	$I_{H_2O}{}^b$	A_J	r_K	$Log(L_{bol}/L_\odot)$	$M/M_\odot$	Age [yr]
CCE98 1	···	M0	1.2	···	+0.52	0.28	$< 1 \times 10^5$
CCE98 2	···	M0	1.0	···	+0.50	0.28	$< 1 \times 10^5$
CCE98 5	···	M1	2.0	···	+0.15	0.275	1×10^5
CCE98 8	···	M1	3.9	···	−0.26	0.38	8×10^5
CCE98 12	···	M0	4.1	−0.26	−0.19	0.40	8×10^5
GK2001 3	···	···	···	···	···	···	···
CCE98 14	···	M0.5	4.0	+0.33	−0.20	0.38	7×10^5
CCE98 16	···	M1	1.2	···	+0.14	0.275	1×10^5
CCE98 17	M0	M0.5	2.7	−0.15	+0.15	0.295	1×10^5
CCE98 18	M1.5	M0.5	4.4	−0.28	+0.11	0.275	1×10^5
CCE98 19	M3	M2	2.9	−0.27	−0.31	0.17	1×10^5
CCE98 21	M3	M2.5	4.3	−0.18	−0.60	0.18	7.5×10^5
CCE98 23	M0.5	M1	8.6	+0.1	+0.10	0.275	1×10^5
CCE98 24	M2	M2	5.9	−0.2	−0.15	0.22	1×10^5
CCE98 25	···	M0.5	1.8	−0.2	+0.61	0.25	$< 1 \times 10^5$
CCE98 26	···	···	···	···	···	···	···
CCE98 27	···	···	···	···	···	···	···
GK2001 18	···	M6.5	0.8	+0.1	−1.74	0.04	5×10^5
CCE98 32	···	M2	3.4	+0.3	+0.34	0.17	$< 1 \times 10^5$
CCE98 33	···	M0.5	4.9	−0.1	−0.06	0.34	4×10^5
CCE98 34	···	M1	4.8	−0.1	+0.48	0.235	$< 1 \times 10^5$
GK2001 21	···	···	···	···	···	···	···
GK2001 24	···	···	···	···	···	···	···
ISO-ChaI 177	···	M3	0.7	+0.2	−1.40	0.225	8×10^6
CCE98 36	···	M0.5	3.1	···	−0.86	0.60	1.5×10^7
CCE98 37	···	M1	2.7	−0.2	−0.41	0.41	1.5×10^6
PMK99 IR Cha INa1[c]	···	M3.5(M6.5)	6.3(6.15)	0.7(0.52)	−1.25(−1.36)	0.19(0.06)	$4 \times 10^6(4 \times 10^5)$
PMK99 IR Cha INa2	···	···	···	···	···	···	···
CCE98 42	···	M2	2.9	−0.2	+0.16	0.185	$< 1 \times 10^5$
CCE98 43	M2	M0.5	4.3	−0.3	−0.85	0.37	4×10^6
CCE98 47	M0	M0	2.8	−0.1	−0.16	0.40	7×10^5
PMK99 IR Cha INa3	···	···	···	···	···	···	···
PMK99 IR Cha INa4	···	···	···	···	···	···	···
CCE98 48	M0.5	M1.5	1.9	+0.1	0.125	0.275	1×10^5
CCE98 49	M4	M5	2.7	−0.1	−0.77	0.12	2.5×10^5
GK2001 42	···	···	···	···	···	···	···
CCE98 50	···	M2.5	1.9	···	+0.35	0.155	$< 1 \times 10^5$
CCE98 51	···	M0.5	2.3	−0.2	−0.10	0.35	5×10^5

[a] Q-index-derived $M_{sub-type}$.

[b] I_{H_2O}-index-derived $M_{sub-type}$.

[c] Values in brackets are corrected due to the high veiling of this object, assuming a M6 spectral type.

Table 8. Previously known young stellar objects: Near-infrared spectral types and derived parameters

Name	Q	I_{H_2O}	A_J	r_K	$Log(L_{bol}/L_\odot)$	$M/M_\odot$	Age [yr]
BYB 18	···	M4	0.5	0.0	−0.99	0.155	2×10^6
Cha IR Nebula	M4.5	M5.5	3.2	0.0	+0.32	0.11	$< 1 \times 10^5$
HJM C 1-6	···	M1	4.1	+0.3	+0.36	0.205	$< 1 \times 10^5$
HJM C 7-2	M0.5	M0.5	2.4	−0.1	−0.03	0.385	7×10^5
HJM C 1-25	M2	M1.5	4.4	+0.1	+0.015	0.19	$< 1 \times 10^5$
Hn 10	M3	M3	1.8	0.0	−0.50	0.17	3×10^5
BYB 43	M1.5	M3	2.5	+0.1	−0.50	0.17	3×10^5
HJM C 1-2	···	M1.5	4.7	+0.3	+0.15	0.225	$< 1 \times 10^5$
HJM C 7-3	M0	M0.5	2.4	−0.2	−0.21	0.345	4×10^5
Hn 11	···	M1.5	2.1	+0.1	−0.10	0.265	2×10^5
ROX 13	···	M1.5	···	···	···	···	···

Table 9. Previously known young stellar objects: Derived parameters

Name	A_J	r_K	$Log(L_{bol}/L_\odot)$	$M/M_\odot$	Age [yr]
Chamaeleon I					
Hn 1	1.0	−0.1	−0.55	0.25	1×10^6
CHXR 73	1.8	−0.1	−0.59	0.80	1.5×10^7
CHXR 74	0.9	−0.1	−0.55	0.72	7×10^6
UY Cha	1.4	−0.1	−0.22	0.275	5×10^5
Hn 6	1.0	−0.05	−0.33	0.60	2.5×10^6
Cha Hα 1	0.1	0.0	−1.88	0.021	$< 1 \times 10^5$
LkHα 332-17	1.2	0.1	+1.22	2.4	2×10^6
BYB 34	0.8	−0.15	−1.08	0.125	1.5×10^6
CHXR 26	2.3	−0.1	+0.06	0.45	4.5×10^5
Cha Hα 2	1.0	0.0	−1.02	0.08	2.5×10^5
HM 15	1.3	+0.1	+0.10	0.30	2×10^5
Cha Hα 3	0.1	0.0	−1.44	0.045	2×10^5
SZ 23	1.8	0.1	−0.47	0.20	3×10^5
HM 16	2.3	+0.3	+0.73	0.35	$< 1 \times 10^5$
VW Cha	0.8	+0.2	+0.61	0.70	2.5×10^5
Glass I	1.5	+0.8	+0.93	0.80	1×10^5
HM 19	0.8	−0.2	−0.67	0.16	7×10^5
Cha Hα 4	0.2	−0.1	−1.29	0.08	7.5×10^5
Cha Hα 5	0.8	−0.1	−1.06	0.09	4×10^5
Cha Hα 6	0.6	−0.1	−1.26	0.05	2×10^5
CHXR 78c	0.6	−0.1	−1.24	0.10	2×10^6
GK-1	0.6	+0.1	−0.25	0.43	9×10^5
BYB 53	0.2	0.0	−0.47	0.45	2×10^6
Lupus					
SZ 65	0.3	+0.1	+0.12	0.32	2×10^5
SZ 68	0.6	+0.15	+0.97	1.5	2×10^5
SZ 77	0.3	+0.1	−0.01	0.335	4×10^5
SZ 82	0.2	+0.1	+0.21	0.31	1×10^5
SZ 128	0.6	+0.2	−0.58	0.35	2×10^6
HO Lup	0.6	+0.2	−0.11	0.33	5×10^5
SZ 90	0.9	+0.2	−0.16	0.40	8×10^5
SZ 94	0.1	+0.0	−1.06	0.16	2×10^6
SZ 96	0.5	+0.1	−0.23	0.28	6.5×10^5
HK Lup	0.6	+0.3	+0.09	0.33	3×10^5
SZ 103	0.8	+0.15	−0.89	0.15	1.5×10^6
Eggen 2	0.2	+0.0	−0.15	0.33	7×10^5
SZ 114	0.6	+0.0	−0.43	0.135	1×10^5
SZ 117	1.0	+0.0	−0.44	0.24	8×10^5
SZ 123	0.45	+0.1	−0.64	0.50	4×10^6
SZ 119	0.3	−0.1	−0.53	0.135	2×10^5
SZ 121	0.6	0.0	−0.34	0.17	1.5×10^5
SZ 122	0.5	−0.1	−0.65	0.25	1.5×10^6
SZ 124	0.0	+0.1	−0.48	0.51	2.5×10^6
Other clouds					
RX J0842.4-8345	0.1	0.0	−0.02	0.44	1.5×10^6
RX J0844.8-7846	0.1	+0.1	+0.11	0.48	4×10^5

Table 9—Continued

Name	A_J	r_K	$Log(L_{bol}/L_\odot)$	$M/M_\odot$	Age [yr]
RX J0915.5-7608	0.0	+0.1	−0.04	0.68	7.5×10^5
RX J0951.9-7901	0.1	0.0	+0.43	1.5	7×10^6